THE UNIVERSITY OF ALBERTA

RELEASE FORM

NAME OF AUTHOR SHANG-CONG CHENG

TITLE OF THESIS **A PHOTODIODE PARALLEL-DETECTION SYSTEM FOR ELECTRON ENERGY-LOSS SPECTROMETRY**

DEGREE FOR WHICH THESIS WAS PRESENTED **MASTER OF SCIENCE**

YEAR THIS DEGREE GRANTED FALL 1983

THE UNIVERSITY OF ALBERTA

A PHOTODIODE PARALLEL-DETECTION SYSTEM FOR ELECTRON ENERGY-LOSS SPECTROMETRY

by

SHANG-CONG CHENG

A THESIS

SUBMITTED TO THE FACULTY OF GRADUATE STUDIES AND RESEARCH

IN PARTIAL FULFILMENT OF THE REQUIREMENTS FOR THE DEGREE

OF MASTER OF SCIENCE

DEPARTMENT OF PHYSICS

EDMONTON, ALBERTA

FALL 1983

THE UNIVERSITY OF ALBERTA

FACULTY OF GRADUATE STUDIES AND RESEARCH

The undersigned certify that they have read, and recommend to the Faculty of Graduate Studies and Research, for acceptance, a thesis entitled **A PHOTODIODE PARALLEL-DETECTION SYSTEM FOR ELECTRON ENERGY-LOSS SPECTROMETRY** submitted by SHANG-CONG CHENG in partial fulfilment of the requirements for the degree of MASTER OF SCIENCE.

Abstract

As in any field of spectrometry, the data collection and recording system of an Electron Energy Loss Spectrometer plays an important role in determining the ultimate performance of the system. In this paper two different detection methods in EELS (serial and parallel) have been reviewed and evaluated in terms of the detection quantum efficiency and linear dynamic range. Parallel detection systems using a semiconductor array as a detector have significant advantage over the serial detection systems. Important properties of the array are presented together with a description of the circuitry needed for interfacing the output to a multichannel analyzer. The advantages and problems of direct and indirect exposure of an array to the electron beam are discussed. Experimental results on the damage to a photodiode array during direct irradiation are presented and discussed. Finally, designs for a post-spectrometer lens system which can be incorporated into the parallel detection system in order to increase the energy resolution are presented. A design for a serial+parallel-combination detection system (which may be used to study the extra-high-energy-loss spectrum) is proposed.

Acknowlegement

I wish to express my sincere gratitude to Dr. R. F. Egerton, my research supervisor for his encouragement and help during this project.

It is a pleasure to thank the members of my supervisory committee (Drs. S. S. Sheinin, E. Pinnington, F. L. Weichman and G. Horlick) for reading my thesis and for their suggestions.

I would also like to thank Mrs. R. Nelson for her typing of mathematical equations.

Finally I am thankful to the Department of Physics for the award of a teaching assistantship.

Table of Contents

Page

1. METHODS OF ELECTRON DETECTION 1

1.1 INTRODUCTION 1

1.1.1 CHARACTERISTICS OF THE ELECTRON ENERGY LOSS SPECTRUM 1

1.1.2 BASIC REQUIREMENTS FOR DETECTORS 6

1.2 SERIAL DETECTION 11

1.2.1 METHOD 11

1.2.2 SEMICONDUCTOR DETECTORS 14

1.2.3 SCINTILLATOR DETECTORS 16

1.3 PARALLEL DETECTION 19

1.3.1 ADVANTAGES OF PARALLEL DETECTION 19

1.3.2 PHOTOGRAPHIC PLATE 21

1.3.3 PARALLEL-RECORDING SEMICONDUCTOR DETECTORS 24

2. PARALLEL RECORDING PHOTODIODE-ARRAY DETECTION SYSTEMS IN EELS 26

2.1 PROPERTIES OF A SELF-SCANNING PHOTODIODE (SSD) ARRAY 27

2.1.1 PRINCIPLE OF OPERATION 27

2.1.2 READOUT NOISE AND DYNAMIC RANGE 32

2.2 DIRECT EXPOSURE TO ELECTRONS 36

2.3 INDIRECT EXPOSURE TO ELECTRONS 38

3. RADIATION DAMAGE TO THE PHOTODIODE ARRAY 44

3.1 INTRODUCTION 44

3.2 EXPERIMENTAL 45

3.2.1
PHOTODIODE ARRAY 45

3.2.2
COOLING DEVICE 46

3.2.3
ANNEALING DEVICE 48

3.3 PROPOSED DEFINITION OF THE OPERATIONAL LIFETIME OF A DIRECTLY-EXPOSED ARRAY 48

3.4 RESULTS AND DISCUSSION 50

3.4.1
THE LIFETIME OF AN ARRAY AT ROOM TEMPERATURE 50

3.4.2
EFFECT OF TEMPERATURE 54

3.4.3
ANNEALING OF AN ARRAY 56

3.5 CONCLUSIONS 57

4. SOME DESIGNS FOR A PHOTODIODE-ARRAY DETECTION SYSTEM .58

4.1 DESIGNS FOR A POST-SPECTROMETER LENS SYSTEM ..58

4.1.1
INTRODUCTION 58

4.1.2
THE DESIGN OF A DOUBLE SYMMETRIC ELECTRON MAGNETIC LENS SYSTEM 62

4.1.3
THE DESIGN OF A SINGLE MAGNETIC QUADRUPOLE LENS 68

4.1.4
THE DESIGN OF A QUADRUPOLE DOUBLET LENS ..75

4.2 A SERIAL-PARALLEL COMBINATION DETECTING SYSTEM 77

4.2.1
INTRODUCTION 77

4.2.2
BASIC DESIGN 81

5. CONCLUSIONS 86

Bibliography 90

List of Figures

Figure — Page

1.1 The geometry of EELS in the electron microscope, illustrating the scattering angle θ, the spectrometer collection angle α and the incident beam convergent angle β.....3

1.2 Energy loss spectra of carbon obtained with an 80kev incident beam and two values of α 4

1.3 Illustration of multiple scans along the same line in the sample; A and B represent two arbitrarily chosen points of interest.....10

1.4 Serial detection by electron counting or via a voltage/frequency converter, using a Tracor Northern 1710 multichannel analyser.....12

1.5 Serial detection by the variation of the output of an auxiliary programmable voltage calibrator, which modifies the primary electron energy before the specimen.....13

1.6 General form of the density/exposure (D/E_x) relation for electron exposure in an emulsion layer.....22

2.1 A simplified schematic of the integration circuit of a N-element SSD array.....28

2.2 A photograph of the Reticon 1024-element array with the control circuit board.....31

2.3 Readout noise N and dynamic range DR, for m readouts signal-averaged over a total recording time τ.....34

2.4 Dynamic range DR and DRE, Detection Quantum Efficiency at the lower dynamic limit DQE as a function of the number of readouts at -30 °C.....39

2.5 Schematic diagram of an EELS indirect-exposure parallel collection system.....41

3.1 The arrangement used to cool an RL-1024S array during exposure to 100 keV electrons.....47

3.2 The arrangment used for annealing an array.....49

3.3 Increase in the leakage current of diodes in an RL-1024S array which was exposed to a 100 keV electron beam at 27 °C. The beam intensity corresponded to 50% saturation.....52

3.4 Cross section of a silicon diode before and after irradiation.....53

3.5 Temperature dependence of the radiation-induced leakage current, measured by operating the array (and circuit board) at several ambient temperatures.....55

4.1 General optics of a magnetic spectrometer.....60

4.2 Magnetic field strength distributions for an iron-free lens, and for coils with an outer magnetic casing.....65

4.3 Cross section of a double, symmetric magnetic lens system.....67

4.4 Photograph of the rotation-free lens system made of a double symmetric magnetic lens.....69

4.5 Oscilloscope tracing of the spectrum of Al, obtained with the incorporation of the designed post-spectrometer lens and a SSD array detector.....70

4.6 Particle trajectories in two planes of a quadrupole lens.....72

4.7 Particle trajectories in two planes of a quadrupole lens pair 76

4.8 Magnification factors *vs* object and image distances for a quadrupole lens pair of separation s = ℓ. 78

4.9 Field strength parameters *vs* object and image distances for quadrupole lens pair of separation s = ℓ. 79

4.10 The design of a serial-parallel combination detection system.....82

4.11 Characteristics curves of the thermoelectric device MI 3040. 84

CHAPTER I

METHODS OF ELECTRON DETECTION

1.1 INTRODUCTION

Electron energy loss spectrometry (EELS) of high energy electrons which have passed through a thin specimen promises to provide a powerful tool, in combination with transmission electron microscopy , for electronic, micro-chemical characterizations of materials. It is particularly desirable for micro-chemical determinations because it complements the already established energy-dispersive X-ray (EDX) spectroscopy by extending detectability from Na down to Li. However, an effective use of electron energy loss spectroscopy for chemical characterization of selected areas in the electron microscope can only be achieved with the development of quantitative detection capabilities. The method of detection is therefore a matter of importance in EELS.

1.1.1 CHARACTERISTICS OF THE ELECTRON ENERGY LOSS SPECTRUM

In EELS, all the information that can be obtained about the specimen is contained in the angular and energy distribution of the electrons that have passed through it, as shown in Fig. 1.1.

By studying these distributions, which result from interactions between the electrons and the specimen, and analyzing them in terms of an appropriate model, the

required information can be found. The most general way to characterize these interactions is to measure the momentum changes suffered by the electrons as they pass through the sample. This is done by measuring both the angle θ through which an electron is scattered, and E, the change in energy relative to the incident energy E_i (Fig. 1. 1). Usually, however, it is sufficient to collect all transmitted electrons lying within a cone of some width α about the incident-beam direction, and to analyze these for their energy loss. Although this approach destroys information about the momentum transfer, since the spectrometer is now integrating information from the whole angular range which it is accepting, it is the one most generally used. The information produced can be readily related to the important properties of the material by simple mathematical models of the interactions (Egerton 1978). The result obtained from such an experiment is an Electron Energy Loss Spectrum in which the transmitted signal intensity J(E) is plotted as a function of the energy loss E for all the electrons scattered within the angular cone α accepted by the spectrometer.

Typical electron energy loss spectra recorded from a thin foil of carbon using 80 keV incident electrons and with α = 100 mrad and α = 10 mrad, respectively, are shown in Fig. 1. 2. The important features of EEL spectra (Fig. 1.2) are as follows. First, there is a large maximum in the intensity centered at E = 0, which is usually called the

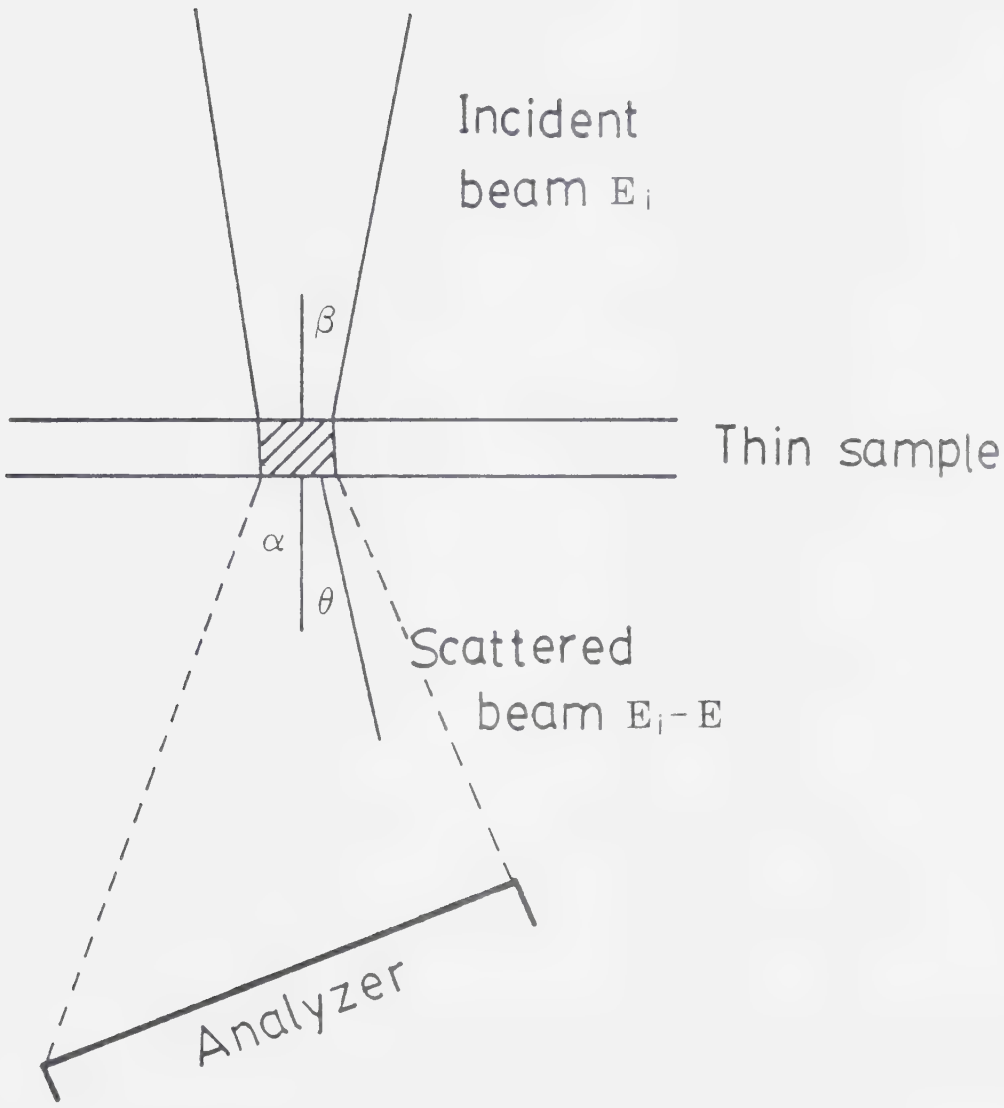

Figure 1.1 The geometry of EELS in the electron microscope, illustrating the scattering angle θ, the spectrometer collection angle α and the incident beam convergent angle β.

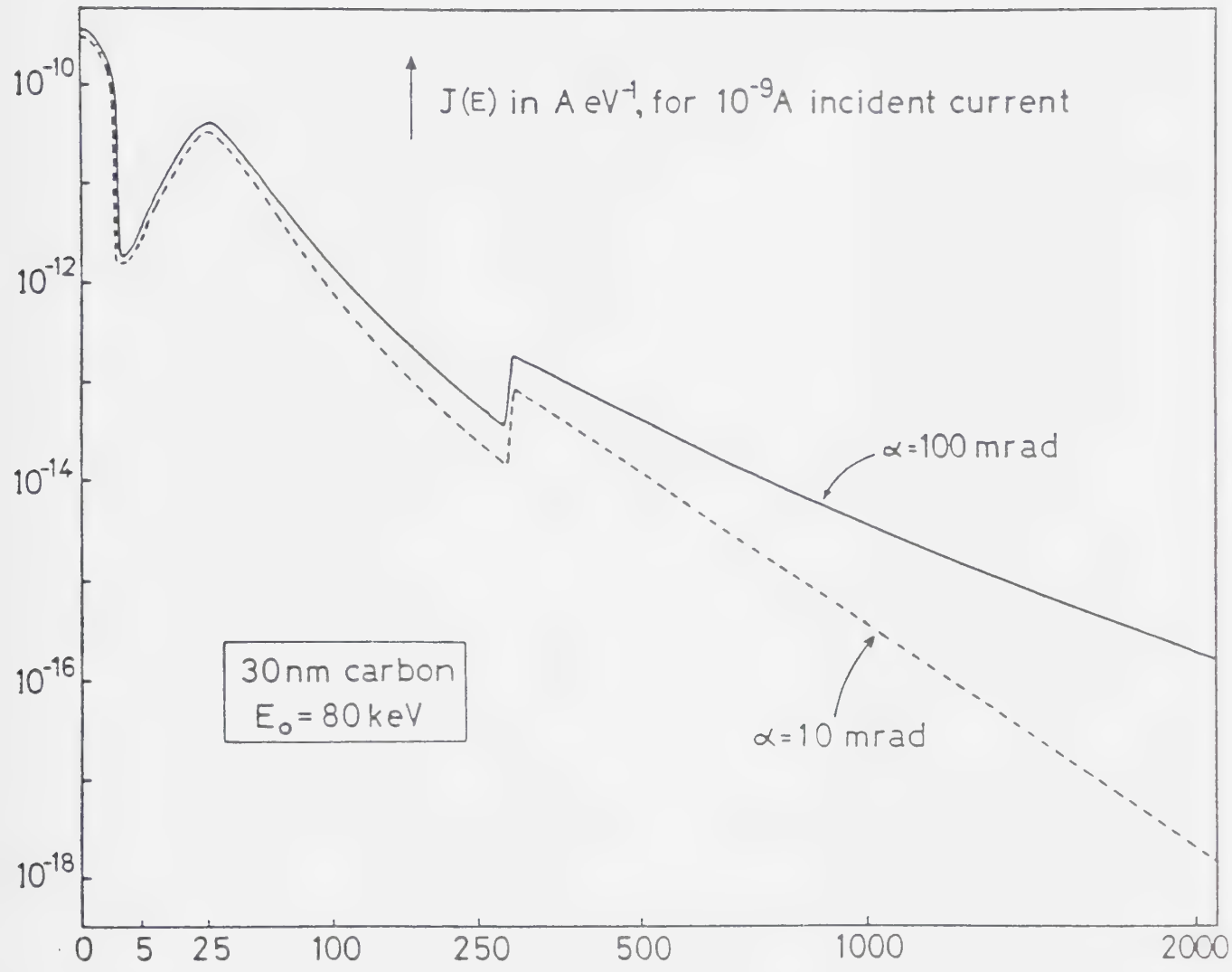

Figure 1.2 Energy loss spectra of carbon obtained with an 80kev incident beam and two values of α .

"zero-loss peak". The zero-loss peak contains both unscattered electrons and electrons which have interacted with the sample without losing significant amounts of energy. In any specimen from which a useful EEL spectrum can be obtained, this zero-loss peak will always be the largest single component. Secondly, there are one or more peaks in a region extending from the edge of the zero-loss peak out to about 50 eV, which is conveniently called the "low-loss" region. The low-loss peaks are due to the interaction of transmitted electrons with valence or conduction electrons of the sample, resulting in plasmon and/or single-electron excitation. Thirdly, the spectrum lying above 50 eV has the general form of a rapidly falling "background", on which are superimposed edges with various features. The characteristic edges in this high-loss region are due to the interaction of the transmitted electrons with inner-shell electrons, resulting in the excitation of inner-shell electrons to various unoccupied states above the Fermi level. The rise in intensity (i.e. an "edge") occurs just above $E = E_k$, where E_k is the appropriate binding energy or ionization energy for an atomic shell k (k representing the type of shell: K, L, M etc.). Therefore, this portion of the EEL spectrum is most important for chemical characterization of specimens, as the binding energy or ionization energy of an edge is a unique property of the element from which it arose. Also, a study of the edges can yield electronic and structural data about the sample. However, as shown in Fig. 1.2, by the time

an energy loss of 250 eV is reached (for this specimen) the signal has fallen by a factor of about 100 times. In fact, edge signals in the high-loss region of a spectrum of a specimen are several orders of magnitude lower than in the low-loss region, because of the small cross-sections in inner-shell excitations. This dramatic fall in intensity after the zero-loss peak and the low-loss peaks is a feature of all energy loss spectra. Since quantitative chemical analysis involves fitting, extrapolating and subtracting the background at each edge and the accuracy of these operations depends, to a large degree, on the noise level in the recorded spectrum, this large range of intensities presents difficulties in both the detecting and the analysis of the spectra.

1.1.2 BASIC REQUIREMENTS FOR DETECTORS

As mentioned above, the signal to be detected in EELS is an electron beam with an energy typically in the 60 to 100 keV range. The peak current is as high as 1000 pico amps. Also, since the signal intensity falls rapidly with increasing energy loss, it is necessary for the detector to be able to monitor currents as low as 10^{-5} pico-amps in order to resolve edge structures. In the case of a high energy K edge, for example, the silicon K-edge at 1839 eV, a dynamic range of 10^5 to 1 relative to the low-loss region may be required to observe edge structure above background (Maher 1979). Furthermore, the beam itself is of strongly

ionizing radiation and can inflict severe damage on detectors sensitive to radiation effects. Therefore, a suitable detector must combine high efficiency (i.e. high sensitivity with low noise), a wide linear dynamic range and an immunity to beam-induced deterioration.

The efficiency of the detector can be specified in terms of the Detective Quantum Efficiency (DQE) (Jones 1959) which is defined as the square of the ratio of the experimentally obtained signal to noise ratio to the signal to noise ratio which would have been obtained with a perfect detector:

$$DQE = \frac{(S/N)^2_{exp}}{(S/N)^2_{per}} \qquad (1.1)$$

The DQE, which is always less than unity, is a measure of the efficiency with which the detector uses the electrons reaching it. The "perfect" detector would add no noise to the incident beam and use every electron incident upon it. If an average number $\bar{n}$ of electrons strike this perfect detector per unit time, then the actual number reaching the detector in any given interval will follow a Poisson distribution with mean $\bar{n}$. The signal-to-noise ratio from the ideal detector would then be the number of incident quanta $\bar{n}$ divided by the inherent shot noise of the beam $\sqrt{\bar{n}}$, thus

$$S/N = \frac{\bar{n}}{\sqrt{\bar{n}}} = \sqrt{\bar{n}} \qquad (1.2)$$

a result often expressed by the statement that the detector is "shot-noise limited".

It is sometimes more convenient to consider the detector and its associated electronics as a combination (Everhart et al 1959). If the bandwidth of the complete system is B(Hz), then the inherent beam noise I_n for an incident current I_i is:

$$I_n = \sqrt{2 \cdot e \cdot I_i \cdot B} \qquad (1.3)$$

where e is the electronic charge. The signal to noise ratio of the beam, as measured by an ideal detector of this bandwidth B, is then

$$S/N = \sqrt{\frac{I_i}{2eB}} \qquad (1.4)$$

The DQE will control the ultimate sensitivity of a detector.

The dynamic range depends on the lower dynamic limit S_{min} and the upper dynamic limit S_{mx}. Thus:

$$DR = \frac{S_{max}}{S_{min}} \qquad (1.5)$$

The low dynamic limit is often based on the study (Rose 1948) of the ability of observers to detect contrast between two points in a scanned TV image in the presence of noise. It was found that for the average observer to discern the difference between two points, the change in the signal ,

ΔS, had to exceed the noise by a factor of 5 (Fig. 1.3):

$$\Delta S \geq 5N \tag{1.6}$$

Therefore, the minimum acceptable signal/noise ratio F in the output of EEL spectrum in normally taken as 5, and we have:

$$S_{min} = F \cdot N = 5N \tag{1.7}$$

There are two possible ways to record the EEL spectrum. Firstly, as a serial operation, by placing a defining slit in the image plane followed by a detector and scanning the dispersion across the slit. Alternatively, the spectrum can be obtained in a parallel operation by putting a detector with spatial resolution in the image plane. In either operation, the detection sensitivity of the spectrometer system, for a given set of electron-optical parameters, will be determined by the performance of the detector and its associated electronics, and its efficiency is therefore a matter of importance. The characteristics of detector systems in serial and parallel operation will be discussed in the following two sections.

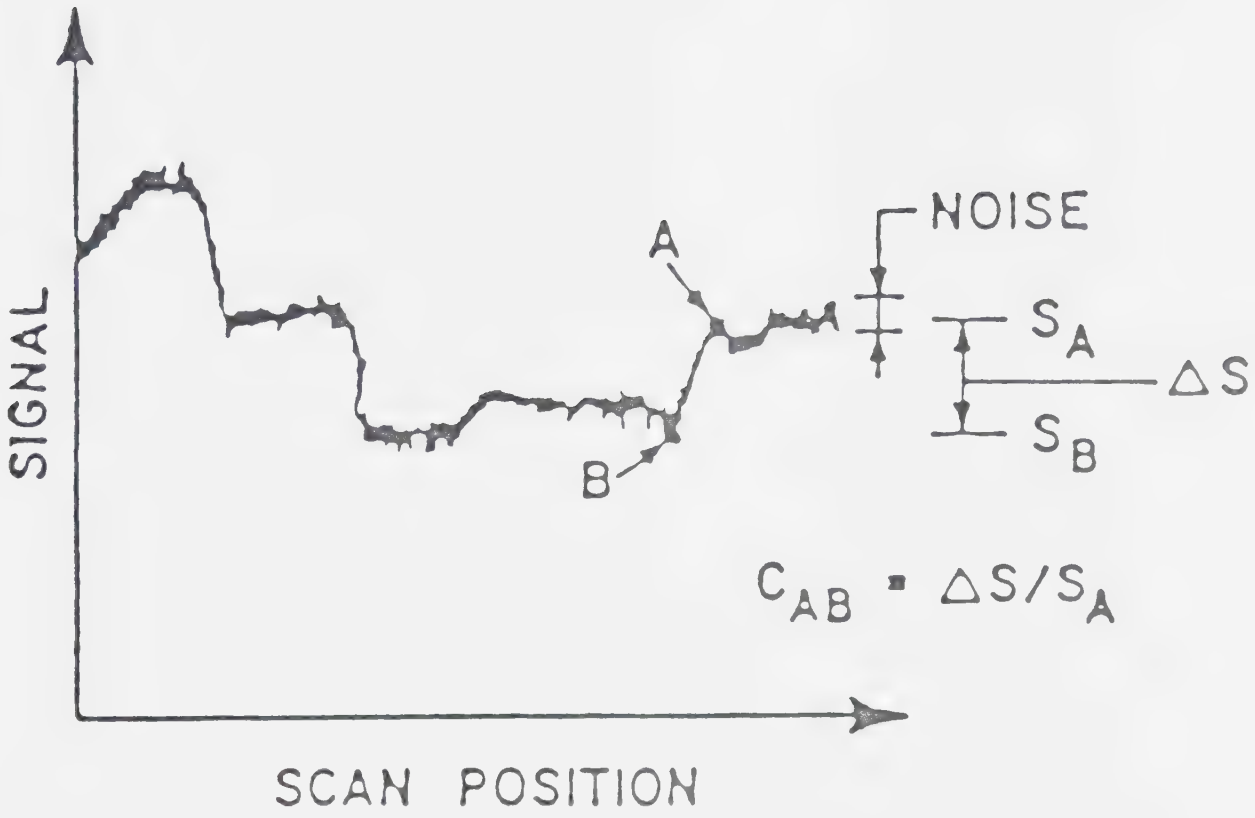

Figure 1.3 Illustration of multiple scans along the same line in the sample; A and B represent two arbitrarily chosen points of interest.

1.2 SERIAL DETECTION

1.2.1 METHOD

Most serial detection of the EEL spectrum is accomplished by scanning the energy-dispersed electrons across a defining slit, either by ramping the spectrometer or through the use of a separate set of scan coils (Fig. 1.4). Sometimes, however, the system has been designed so that the energy is changed before the spectrometer. This is achieved by a variation (between 0 and 1000 v) of the output of an auxiliary programmable voltage calibrator (Trebbia 1977), which modifies the primary electron energy before the specimen as shown in Fig.1.5.

Although the spectrum can be recorded for analysis by displaying it on a chart recorder, the best technique is to store the spectrum in a multi-channel analyzer (MCA). This is because that the MCA can accommodate a relatively wide dynamic range, and once the spectrum has been collected, it can be processed either directly or with a computer.

There are several ways to digitise the detector output for storage in MCA. Firstly the detector can be run in a "pulse-counting" mode, with a suitable amplifier and discriminator being used to shape the pulses for acceptance by the MCA. Alternatively, the detector can be used as an analog device and its output digitized by the use of a voltage to frequency V/F converter (Joy and Maher 1980) or through an analog to digital A/D converter (Egerton and

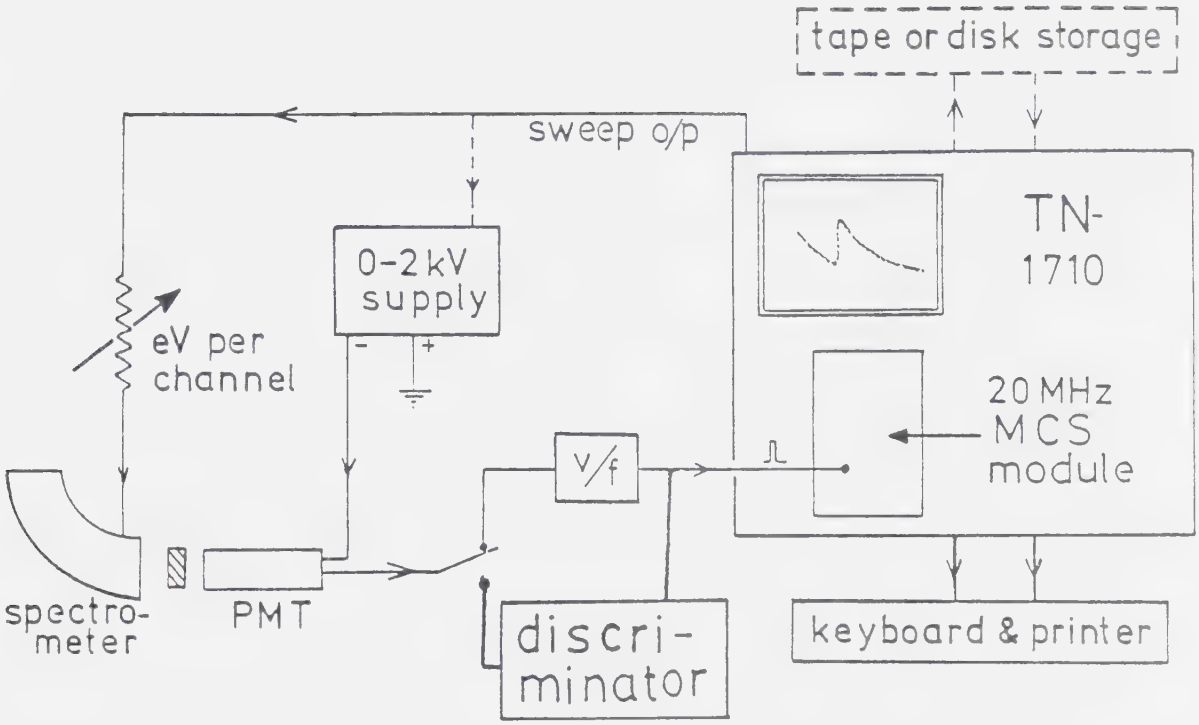

Figure 1.4 Serial detection by electron counting or via a voltage/frequency converter, using a Tracor Northern 1710 multichannel analyser.

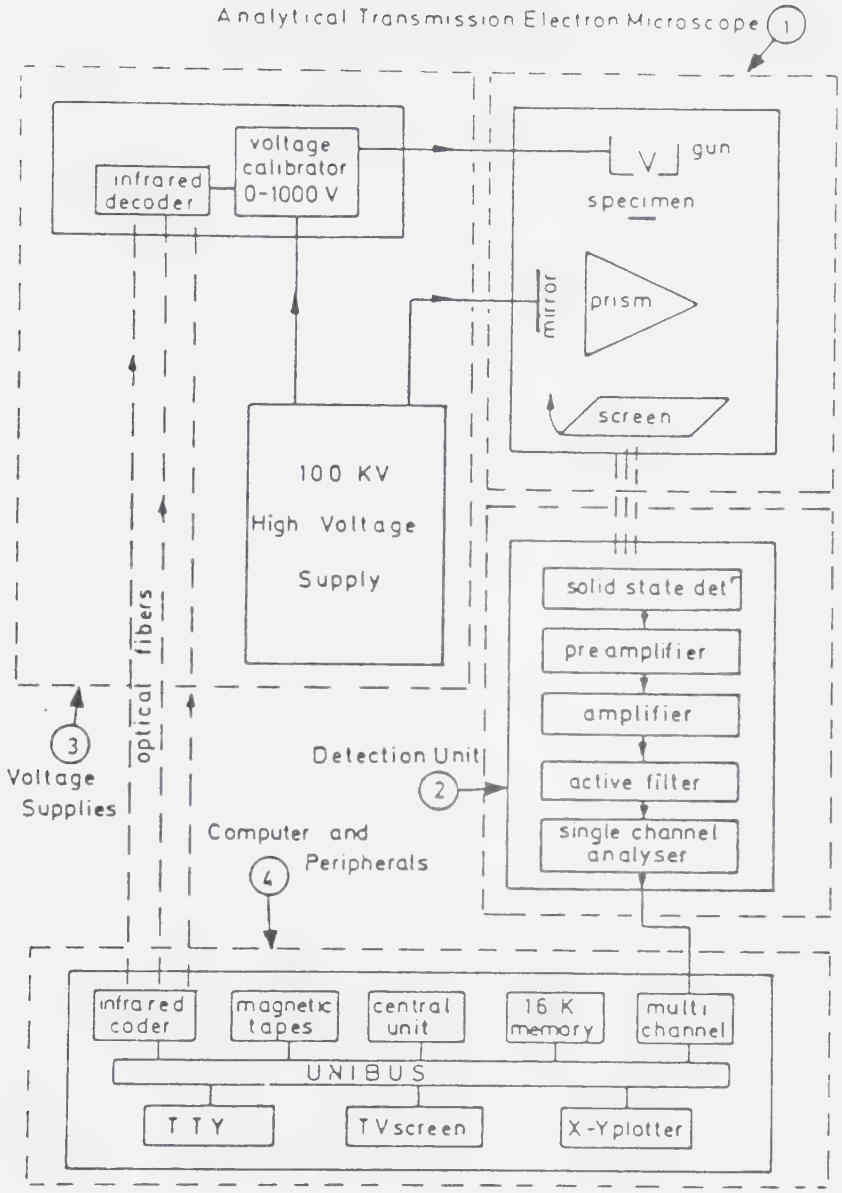

Figure 1.5 Serial detection by the variation of the output of an auxiliary programmable voltage calibrator, which modifies the primary electron energy before the specimen.

Kenway 1979). In principle the pulse counting approach is superior because the result is essentially independent of the gain of the detector, and contains no component due to dark current signals from the detector (assuming, in both cases, that the discriminator is properly set up). This approach therefore can detect very low signals.

Direct digitization of the analog output of a detector is straightforward; but A/D converters with greater than 16 bit precision are expensive and there is thus a limit to both accuracy (2 part in 10^5) and the dynamic range of the result that can be obtained in this way. Voltage to frequency converters are relatively cheap and current commercial 10MHz units, when carefully set up, offer a precision equivalent to a 19 bit A/D converter together with a dynamic range in excess of 10^5. Thus they can easily cope with the zero-loss region. However such units generate a substantial dark-current count which must be stripped from the spectrum before analysis. In either case, the accuracy of the result obtained will depend on the gain stability of the detector and its associated electronics, and there can be significant errors due to (even transient) overloading of any part of the signal chain.

1.2.2 SEMICONDUCTOR DETECTORS

Several workers (e.g. Trebbia et al 1977) have used semiconductor detectors in serial detection of EEL spectrum because of their compactness and efficiency. A single 100

keV electron will produce in excess of 10^4 electron hole pairs. Also, if the depletion depth of a diode at this accelerating voltage is optimally chosen, a large fraction of these carriers can be collected by the action of the internal bias field, giving the device a considerable gain. Even higher collection efficiency can be obtained by biasing the diode; but this also increases the dark current. The DQE of such a detector is $DQE = 1/(1 + E_m/E_i)$, where E_m is the energy to create an electron-hole pair, and E_i is the incident beam energy. At beam energies in the keV range, the DQE is thus very close to unity. The combination of the relatively high impedance and capacitance represented by the detector can be handled effectively by analog amplifiers to give adequate performance under most microanalytical conditions. However, the pulse counting performance is strictly limited, since the internal capacitance broadens the pulse and substantial shaping time is required to ensure accurate discrimination and counting. A typical maximum count rate is only of the order of 10 kHz so that in any reasonably efficient spectrometer, counting operation will only be feasible at high energy losses. The radiation sensitivity of a solid state detector is also a problem in many cases. Reversible damage, manifested by a loss of gain and an increase in dark current is often observed for low radiation doses. High radiation dose can result in a permanent loss of performance.

1.2.3 SCINTILLATOR DETECTORS

Scintillator/photomultipliers are the most used serial detectors because they combine cheapness, speed and efficiency. The scintillator transforms the energy of the primary-electron beam into photon energy. The generated light quanta are detected by a sensitive, spectrally adapted photomultiplier. The DQE of a scintillator detector is thus a function of both the photomultiplier and the scintillator. If, on average, each electron incident on the scintillator produces p electrons from the photocathode, then p has a Poisson distribution and the DQE of the combination is DQE(PM) = 1/(1 + (1/P)). The efficiency of the scintillator, its coupling to the PMT and the quantum efficiency of the photocathode are thus all significant. In theory, a single 100 keV electron could generate thirty thousand 3.3 eV "blue" photons from, for example, the popular NE102 plastic phosphor. However the actual conversion efficiency is only about two percent (Pawley 1974); so only about 600 are produced and of these only about a quarter are travelling in the right direction to reach the photocathode. Since this photocathode has a typical efficiency of about twenty percent, the final yield is about 30 photoelectrons, to give a DQE of 0.97. At lower voltages however the p value and the result DQE can be much worse; and Comins et al (1978) have reported values as low as 0.1. In pulse counting the statistical fluctuations in p will mean that for a specific discriminator setting some "real" events will be eliminated,

leading to a fall in the DQE.

The choice of a scintillator involves requirements of speed, radiation sensitivity and efficiency. For analog systems, where only the radiation sensitivity and efficiency are important, the most popular choices have been plastics, (e.g. NE102), or glasses, such as CaF_2 doped with Europium. Plastic scintillators are a factor of two or three times more efficient than glass scintillators, but they show significant damage with radiation dose, resulting in a rapid loss in efficiency. It has been reported (Oldham et al 1971) that for a plastic scintillator NE102A at a radiation dose of 100 kRads there would be a reduction of an order of magnitude in efficiency, although some of the damage is reversible. The glass scintillators, by contrast, display a high level of radiation resistance with little fall off in efficiency for doses exceeding a thousand MRads (Wiggins 1978), and the damage is reversible on heating in air.

For pulse counting all the parameters of the scintillator must be considered. At 100 keV, any undamaged scintillator is capable of producing pulses sufficiently large to ensure a DQE, after discrimination, which should theoretically be close to unity. The problem is then to find the ideal combination of decay speed and radiation resistance. One satisfactory solution is the use of high efficiency yttrium aluminium garnet (YAG) phosphors doped with rare earths (Blasse and Brill 1967). A commercial example is P-46 (cerium doped YAG) which is available as a

powder. This has a decay time of 20 nano-seconds, allowing a peak count rate of about 20 MHz and an efficiency which is about twice that for NE102. In its powdered form the radiation resistance is good, a dose of some tens of M Rads being required to cause a fifty percent fall in efficiency, but the powder is not stable on repeated exposure to air.

It is worth mentioning a recent, important production of large single crystal scintillators obtained by liquid phase doping of YAG substrates with Cerium, or mixed rare-earths, to produce an active region ten to twenty microns deep. The efficiency of such scintillators is very high and a good spatial resolution and uniformity can be predicted as a result of the complete crystallinity, compared to the case of polycrystalline and powder phosphors where light is reflected at internal faces resulting in a loss of optical resolution and efficiency. More important, they have been found to be exceptionally radiation resistant (Autrata et al 1978). Therefore, their development offers hope of enhanced performance.

The photomultiplier is an excellent component in the measurement of electron-beam intensity, having very good linearity, wide dynamic range, high sensitivity and direct electron output.

In summary the photomultiplier-scintillator combination offers good all-round performance for serial detection. However, no matter what kind of detector is used, the DQE for any form of serial detection is limited. This is because

of the spectrum of N channels, only one is being sampled at any time. If the intensity/channel were constant, the signal/noise ratio of the entire spectrum would be reduced by a factor $1/\sqrt{N}$ (from equation 1.2). So the DQE for a perfect serial detector, compared to that for a perfect parallel detector, must satisfy the inequality:

$$DQE_{(serial)} \leq 1/N \cdot DQE_{(parallel)} \qquad (1.8)$$

Therefore the serial mode of detection, in which information is wasted, is at a considerable disadvantage compared to any form of parallel collection.

1.3 PARALLEL DETECTION

1.3.1 ADVANTAGES OF PARALLEL DETECTION

In EEL spectrum the beam of electrons transmitted through the analyzer is spatially dispersed in the image plane. Parallel readout of the spectrum is therefore possible if an array of detectors, or a single detector with spatial resolution, is placed in this plane. Over the past few years there has been considerable interest in the developement of parallel readouts because of the fundamentally poor DQE of a serial readout of the spectrum, as mentioned in the previous section.

A comparison between parallel and serial detection can be made as follows. If the width of the slit of the

spectrometer in serial detection is ΔX , the dispersive power of the spectrometer is **d** and the energy range recorded is E_{mx}, then the fraction of electrons recorded is $n_d = \Delta X/(d \cdot E_{mx})$. The collection efficiency of the detector, n_d, can be improved by an increase in the width of slit, ΔX, but only at the expense of a degradation $\Delta E_d = \Delta X/d$ in energy resolution. For light-element microanalysis, E_d = 5 eV and E_{mx} = 1000 eV are typical values, and yield a detection efficiency n_d = 0.5 %. A parallel detector receives all the electrons simultaneously. If a typical value of the backscattering coefficient is assumed, a detection efficiency of at least 50 % should be possible (Egerton 1981 a). The recorded signal is therefore larger by a factor of about 100 compared to serial detection. If the noise level in the recorded spectrum is assumed to be increased mainly through Poisson statistics of the arriving electrons, the signal/noise ratio will be therefore improved by a factor of $\sqrt{(100)} = 10$ in this case, i.e.

$$(S/N)_{parallel} = 10 \cdot (S/N)_{serial}$$

Then applying equation (1.8), We have:

$$DQE_{(parallel)} \geq 100 \cdot DQE_{(serial)} \qquad (1.9)$$

This improvement will in turn make weak inner-shell ionization edges more visible above the background and improve the accuracy of quantitative analysis.

1.3.2 PHOTOGRAPHIC PLATE

A photographic plate placed in the exit focal plane of the spectrometer was the earliest method used to record the electron dispersion. In this method, the whole spectrum is recorded in parallel. For 100 keV electrons the DQE for suitable emulsions is very close to unity (Farnell and Flint 1975) and the plate is nearly an ideal shot-noise limited detector.

The attenuation of light by a developed emulsion layer is expressed quantitatively as the density D. It is defined as the logarithm to the base 10 of the reciprocal of the transmission T, i.e. $D = \log_{10}(1/T)$. Exposure E_t is the product of exposure time and electron density at the surface of the emulsion layer, expressed, for example, in electrons/m^2. The usual shape of the D/E_t curve for electron exposure is shown in Fig. 1.6, and
may be represented approximately by the relation

$$D = D_s(1-e^{-KE_t}) \qquad (1.10)$$

where D_s is the saturation density, and K relates to the size and sensitivity characteristics of the emulsion grains. For small values of E_t, expression (1.10) reduced to

$$D = K \cdot D_s \cdot E_t \qquad (1.11)$$

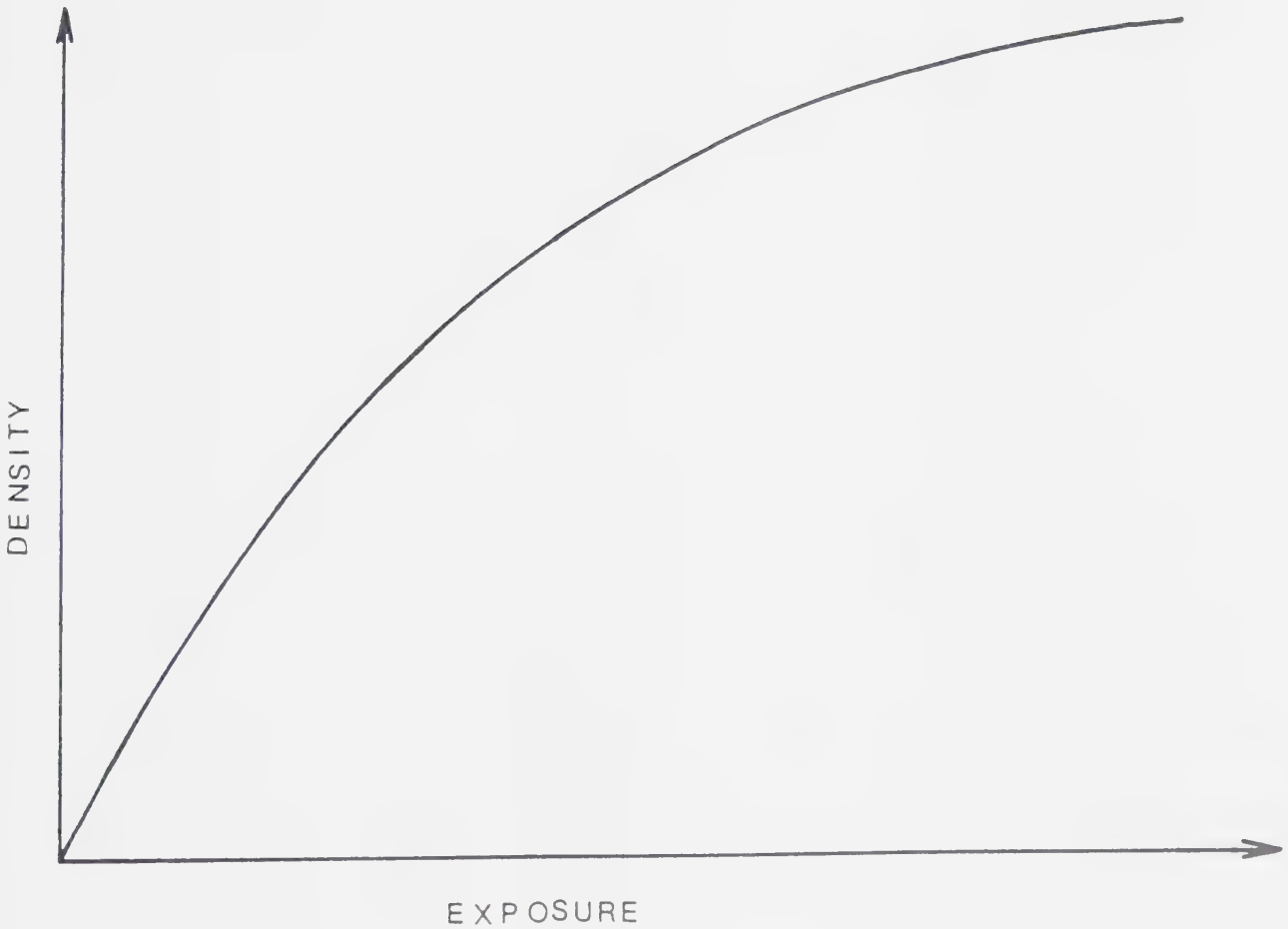

Figure 1.6 General form of the density/exposure (D/E_t) relation for electron exposure in an emulsion layer.

The existence of an initial region to the D/E_t curve as indicated by expression (1.11) is easily appreciated when it is recalled that the usual situation is that one or more grains can be rendered developable by a single electron hit. Since density is proportional to the number of electrons incident per unit area, it follows that D will be proportional to E_t. As exposure is increased, the slope of the D/E_t plot will diminish because the number of grains already rendered developable is such that an increased fraction of the exposure is wasted on such grains. An asympototic approach is made to the saturation density level corresponding to development of all the grains in the layer or, alternatively , of those grains in the layer accessible to electrons (if the electron range is less than the emulsion thickness). In general terms, the linear region of the D/E_t curve extends up to about $D_s/4$. Emulsions typical of those used in electron micrography may have a D_s of about 8.0 for exposure to electrons of 50 keV energy or more, and hence will exhibit proportionality between D and E_t up to densities of about 2.0. In practice, it is virtually impossible with a photographlic plate to record both the low-loss and the core-loss regions of the spectrum in the same exposure.

Photographic techniques also suffer from the fact that subsequent processing is required before the data can be analyzed, and because this processing can itself greatly affect the linearity of the information transfer.

Furthermore, numerical data can only be obtained by performing micro-densitometry on the plate, which is difficult to combine with computer storage.

1.3.3 PARALLEL-RECORDING SEMICONDUCTOR DETECTORS

The parallel-recording detector using a semiconductor device represents an attempt to retain the advantages of PMT and also achieve simultaneous spectral measurement. In this system, the equivalent of an exit slit-PMT combination is mounted at each point in the exit focal plane of the spectrometer. Such systems provide simultaneous detection of a considerable range of the spectrum.

Two main device types have been employed in electron microscopy : the charge-coupled device (CCD) array (e.g. Chapman et al 1982, Downing et al 1980, Roberts et al 1982) and the self-scanned photodiode (SSD) array (e.g. Jones et al 1977, Jenkins et al 1980, Egerton 1981, Shuman et al 1981). Although both devices rely on the generation of electron-hole pairs by the incoming electron or photon, they differ in the way that this information is readout from the detector.

The CCD or SSD could either be used directly to detect electrons or, alternatively, be exposed indirectly, where the electrons are converted into photons at a transmission or reflection phosphor. Since the spectrum is dispersed in a straight line, a linear-array detector can be used. But if equivalent performance can be obtained, there are good

reasons for using a two-dimensional (image) array since this will permit direct inspection of the aberration figure of the spectrometer and, with the addition of a post-spectrometer lens, allow the observation of energy filtered images and diffraction patterns (Shuman and Somlyo 1981).

The detection efficiency, dynamic range and the other performances of CCD and SSD, both exposed directly or indirectly, will be discussed in detail in the next chapter. It will be seen that the use of parallel rather than serial readout has replaced one set of problems and limitations by another. However, the parallel detection schemes do offer a significant, though not yet overwhelming, benefit.

CHAPTER II

PARALLEL RECORDING PHOTODIODE-ARRAY DETECTION SYSTEMS IN EELS

Several types of diode arrays have been developed as described in review articles by Fry (1975) and Lowrance (1979). These diode arrays have been incorporated into optical spectroscopy (Horlick 1976) and X-ray emission spectroscopy (Gamble et al 1979). Among these arrays, two types which have been investigated in the context of microscopy are the self-scanning photodiode (SSD) array and the charge-coupled diode (CCD) array (1.3.3). Both types are available as linear or two-dimensional arrays. And both types combine three basic functional elements (i.e. radiation sensor, charge storage and scanning circuitry for readout) into a single integrated circuit. The discussions in the following sections will focus on the use of a large-aperture SSD array; in particular, the S-series devices containing 128, 256, 512, or 1024 elements available from Reticon Corporation (EG & G Reticon, 345 Potrero Avenue, Sunnyvale, CA 94086, U.S.A.). However the general argument will apply qualitatively to CCD arrays since although they have a somewhat different internal operation and require a different control circuit, their output signal is of similar form.

2.1 PROPERTIES OF A SELF-SCANNING PHOTODIODE (SSD) ARRAY

2.1.1 PRINCIPLE OF OPERATION

The operation of a SSD array involves the operation of the array itself, the control circuit, and the measurement of its "video" output signals.

The SSD array itself is a single integrated circuit containing functions of radiation sensor, charge storage and readout. A simplified schematic of the integration circuit of a N-element array is shown in Fig. 2.1. Its working principle is as follows. Each diode, which is made by diffusing a p-type impurity into the n-type silicon substrate, is connected in series with a field-effect transistor (FET) switch. The FET switches are connected to a common output line and are controlled by a single bit that is shifted through a N-bit shift register. While a particular FET switch is closed by the bit in the shift register, the diode is charged up to its full reverse bias potential (5 V for a Reticon 1024-element array). During an integration period τ, electron-hole pairs will be generated due to thermal excitation (thermal leakage current) and radiation (photons or charged particles). The diode thus discharges at a rate which depends on its internal capacitance and on the irradiation received. After the integration period, the signal necessary to reestablish the reverse bias on the diode is thus a measure of the sum of the electron-beam generation and the thermal leakage current

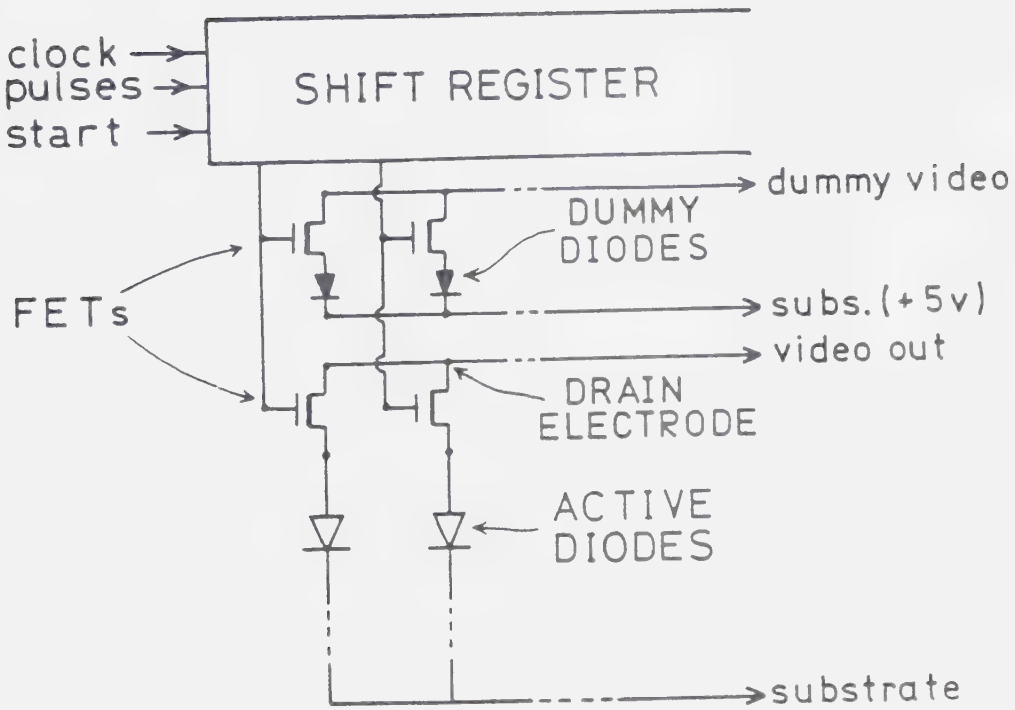

Figure 2.1 A simplified schematic of the integration circuit of a N-element SSD array.

integrated over the integration period. Readout is accomplished by an external control circuit, through the shift register. In this way, a bias signal is applied sequentially to each photodiode, and recharge pulses appear serially at the output as a "video" signal, which is subsequently amplified and processed.

In practice, adjacent diodes (numbered odd and even) are driven by two different shift registers and are connected to separate output lines, but the two outputs can be subsequently combined in the external circuitry. Also, "dummy" diodes incorporated along the array produce their own (odd and even) outputs, which are combined with the output of the active diodes in such a way as to reduce switching transients due to parasitic coupling.

The control circuit contains an oscillator, running at between 10kHz and 10MHz, and an integration counter. The oscillator drives the integration counter, whose initial pulse restarts the first bit of the shift register and so is called the "start pulse". The oscillator also supplies clock pulses which, after the start pulse has been applied, cycles the bit through the shift register reading out the array. The integration time is controlled by the time between start pulses, which depends on the clock frequency and the switch setting at the integration counter. Once a scan is initiated by a start pulse, the complete array must be scanned. Another pulse may be applied immediately after the array has been completely scanned or the start pulse can be delayed

for up to many seconds (if the array is cooled) in order to increase the integration time and so the sensitivity of the detector.

A photograph of the Reticon 1024-element array with its control circuit board is shown in fig. 2.2. For the actual readout of the array, four properly phased clocking signals and a start pulse are generated. The amplifier connected to the video output line of the array contains a sample and hold circuit which produces clean output pulses.

The video output of an array can be viewed directly on an oscilloscope. But for permanent storage or accumulation of data, the output should be fed into a multichannel analyser (MCA). For electronic storage, the output voltage levels have to be converted into digital signals, which can be done using either an analog to digital (A/D) converter or by a voltage to frequency (V/F) converter. However it is necessary to ensure that the information obtained from each diode in the array is placed in the correct MCA channel. In other words, the MCA channel access must be synchronized with the array readout. One way of achieving this synchronization is to feed a beginning-on-line pulse (start pulse) obtained from the array circuit to start the MCA scan, followed by channel-advance pulses at the clock frequency which is one quarter of the oscillator frequency for 4-phase clocking. With the correct synchronization, any desired number of array readouts can be superimposed in MCA memory.

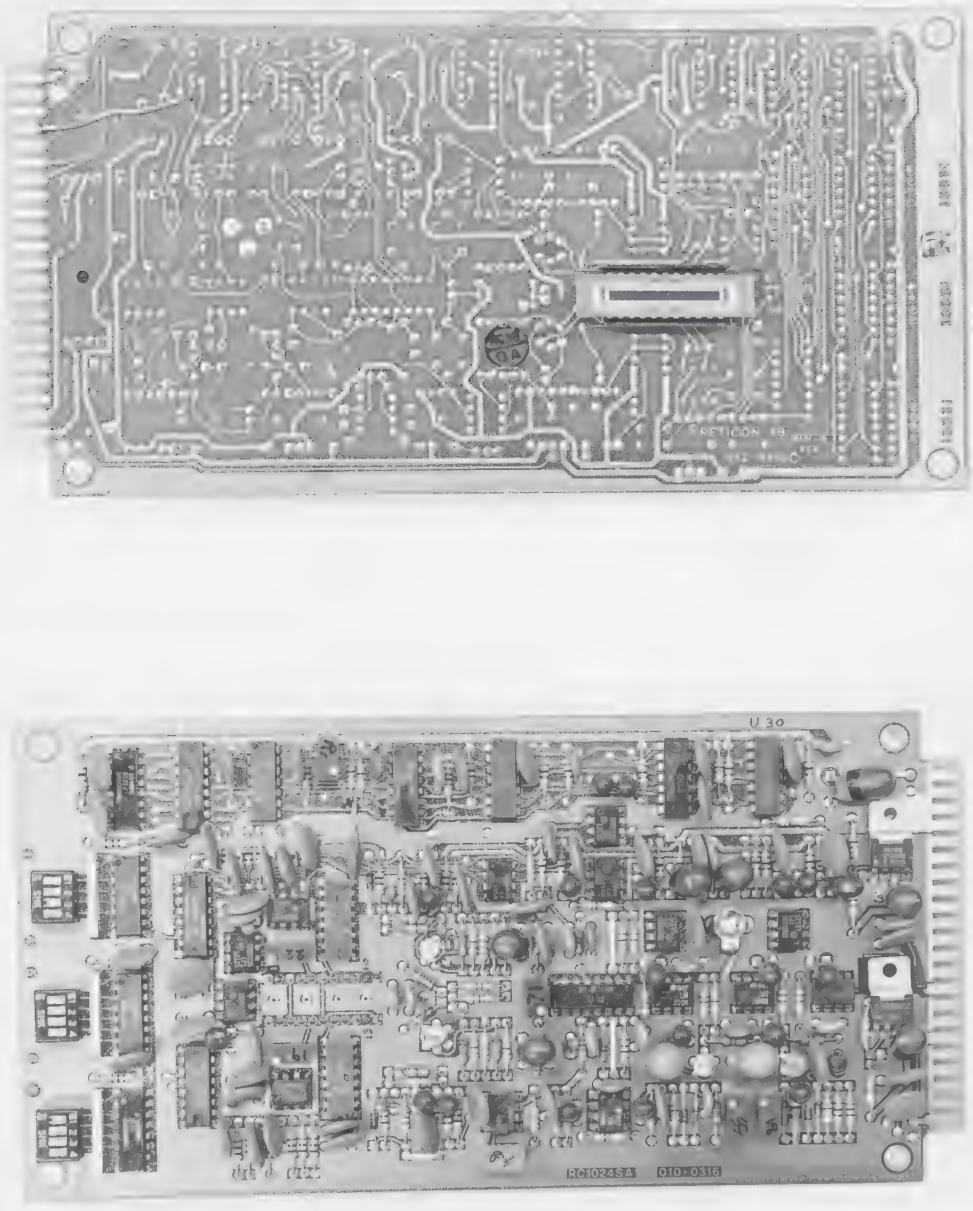

Figure 2.2 A photograph of the Reticon 1024-element array with the control circuit board.

2.1.2 READOUT NOISE AND DYNAMIC RANGE

In addition to the desired signal, the array output contains a certain amount of readout noise. Expressed in terms of an equivalent number of electron-hole pairs generated by the incident radiation, the root-mean-square noise amplitude N_r is given by:

$$N_r = [N_c^2 + N_d^2 + N_a^2]^{\frac{1}{2}} \qquad (2.1)$$

N_c represents diode-reset noise, and is given (Simpson 1979) by:

$$N_c = [2kT(C_d+C_v)/e^2]^{\frac{1}{2}} \qquad (2.2)$$

where k is Boltzman's constant, T is absolute temperature, C_d is diode capacitance, C_v is the video-line capacitance and e is the electronic charge.

N_d represents shot noise due to the thermal leakage current (i.e. dark current) I_d of each diode during the integration period τ and is given by:

$$N_d = [I_d \tau e^{-1}]^{\frac{1}{2}} \qquad (2.3)$$

N_a represents noise introduced during subsequent amplification.

Values of readout noise as function of integration time are given in Fig. 2.3, using data appropriate to the Reticon S-series array (Reticon 1978). It is seen from Eqs.(2.1),

(2.2) and (2.3) that N_r increases with τ but decreases with T due to the shot-noise and the diode-reset noise term.

The maximum detectable output signal corresponds to complete discharge of a diode during the integration period τ, and is given by:

$$S_{max} = (Q_{sat} - I_d\tau)/e \tag{2.4}$$

where Q_{sat} is diode saturation charge and $I_d\tau$ represents the effect of thermal leakage. From Eqs.(1.5) and (1.7) the dynamic range should be:

$$DR = \frac{S_{max}}{S_{min}} = \frac{Q_{sat} - I_d\tau}{eFN_R} \tag{2.5}$$

This quantity is also plotted for a Reticon S-series array in Fig. 2.3. In the case of an array operating at room temperature, the thermal leakage current severely degrades the dynamic range for τ > 1 s; whereas integration times up to at least 100 s can be used if the device is cooled to -30 °C.

The noise figure and dynamic range defined in Eq.(2.1) to Eq.(2.5) apply to a single readout of data. In order to increase the dynamic range, multiple readouts can be used. This is achieved by interfacing the array to an electronic storage device (such as a MCA), increasing the clock rate by an appropriate amount, thereby dividing a given total exposure time τ into m periods, and combining the m separate

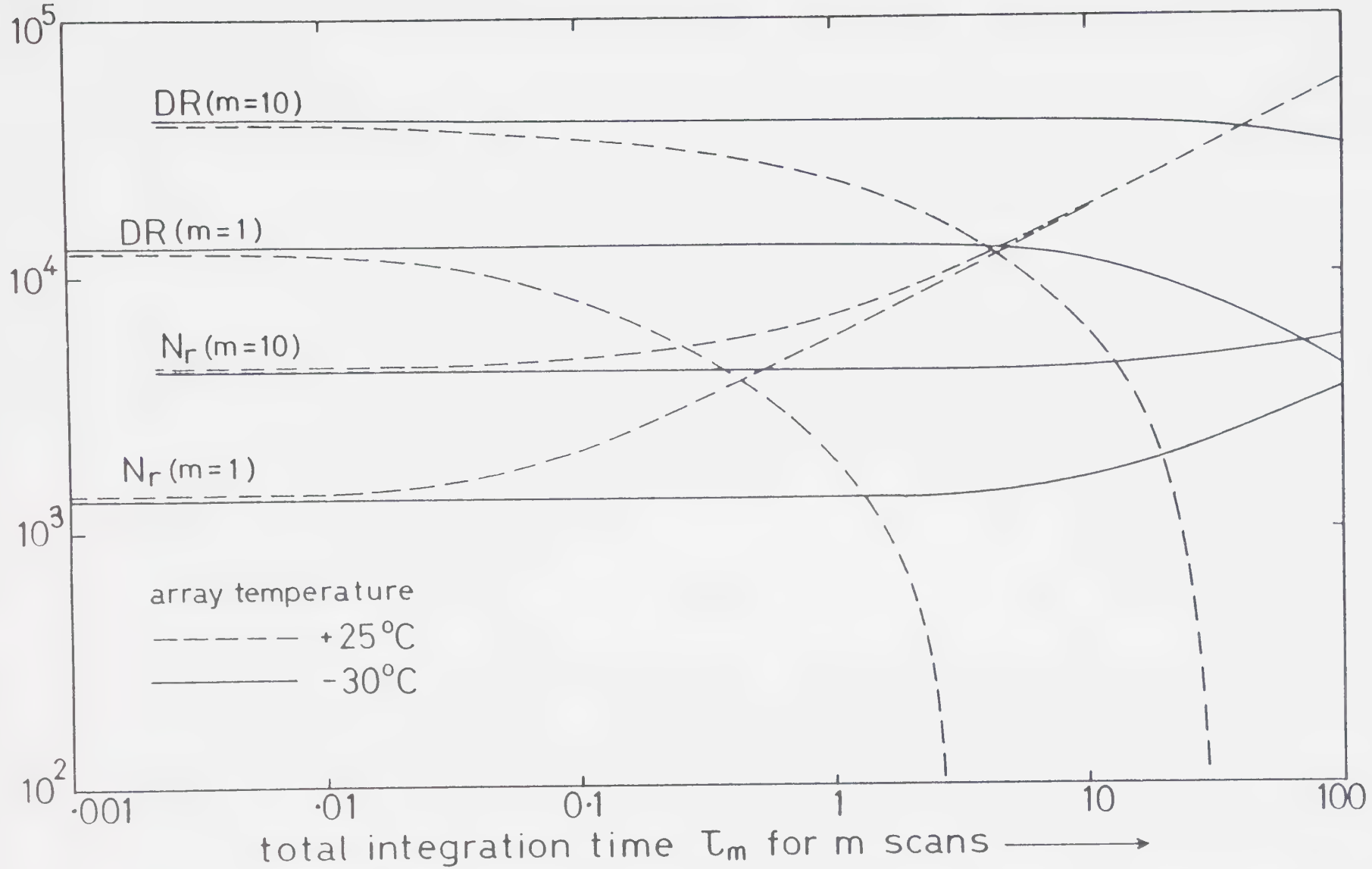

Figure 2.3 Readout noise N_r and dynamic range DR, for m readouts signal-averaged over a total recording time τ.

readouts electronically. The accumulated readout noise is then given by:

$$N_r^2 = (I_d \tau_m)/e + mN_c^2 + mN_a^2 \qquad (2.6)$$

Here the "setup" time required between readouts is ignored, being typically 20 μs or less. Comparing Eq.(2.6) with Eqs.(2.1), (2.2) and (2.3), it is seen that the diode shot noise remains the same as for a single readout since it depends only on the total exposure time, but the accumulated reset noise and amplifier noise are both increased because these noise components contribute to every readout. Consequently, N_r and S_{min} are larger than for a single readout, but by a factor somewhat less than $\sqrt{m}$. On the other hand, S_{max} increases by a factor of m, and the dynamic range will therefore be larger by a factor of at least $\sqrt{m}$ compared to the case of a single readout. The dynamic range and the noise figure for m = 10 is also plotted in Fig. 2.3. The dynamic range (DR) as a function of m is shown in Fig. 2.4 for a total acquisition time of 10 s at -30 °C. A limitation on the dynamic range of the stored data could be the resolution of the digitization device or the storage capacity of each MCA channel. However, in 1000 scans, a 14 bit A/D converter could permit a dynamic range $\simeq 4 \cdot 10^5$ (see Fig. 2.4).

2.2 DIRECT EXPOSURE TO ELECTRONS

Although currently-available diode arrays are designed as photon detectors, they also respond to incident electrons of suitable energy. However, there are important differences. First, each electron will generate several thousand electron-hole pairs. Electrons of energy below 20 keV are largely absorbed in the passivating SiO_2 surface layer. Those of energy above 100 keV have a range (in silicon) which exceeds the hole diffusion length (about 50 μm), and would therefore be detected less efficiently. For energies in the range 30 to 100 keV, electron-hole production results in one electronic charge being lost by a photodiode for each 3.7 eV of energy dissipated. Consequently, a single 80 keV electron will produce a diode signal of about $2.2 \cdot 10^4$ electrons. If the diode is not emptied at sufficiently frequent intervals, problems can be experienced with the diode "saturating". On the other hand, since the output signal is well above the readout noise, particularly for a device cooled below room temperature, a directly exposed array is capable of single-electron sensitivity. Secondly, since the output signal per electron is so large , the dominant source of noise in the output is electron-beam shot noise. Thirdly, under the bombardment of high-energy electrons, the diode and the peripheral circuity are at risk. There is a problem of radiation damage, which increases with the radiation dose received. This problem is the major drawback of direct-exposure to electrons, and a

detailed discussion will be given in Chapter 3.

The dynamic range and the sensitivity for an array directly-exposed to electrons are considered as follows. The total output noise N_t is given by:

$$N_t^2 = N_b^2 + N_r^2 \tag{2.7}$$

Here, N_b is the electron-beam shot noise, equal to $\eta\sqrt{n}$ where n is the total number of incident electrons recorded per diode and η is the number of diode electrons produced per incident electron ($\eta \simeq 22000$ at 80 keV incident energy)

The lower dynamic limit S_{min} according to Eq.(1.7) is

$$S_{min} = \eta\, n_{min} = F\, N_t \tag{2.8}$$

where F is the Rose factor (1.1.2). From Eqs.(2.7) and (2.8) we have

$$n_{min} = F^2[0.5 + \sqrt{0.25 + (N_r/\eta F)^2}] \tag{2.9}$$

where N_r is given by Eq.(2.1).

The upper dynamic limit is set by diode saturation. The maximum signal S_{max} which can be accumulated in m readouts over a total time τ_m is

$$S_{max} = (mQ_{sat} - I_d\tau_m)/e \tag{2.10}$$

The dynamic range DRE for direct electron exposure is shown in Fig.2.4 as a function of m, the number of readouts in a given time τ_m (= 10 s in this case) at -30 °C. For m = 1, DRE is only about 100 (assuming a cooled array, otherwise the leakage current saturates the device in less than 10 s), but increases almost linearly with m so that values in excess of 10^5 become possible with a large number of readouts.

The DQE can be calculated according to Eq.(1.1), and we have

$$DQE = \frac{(\eta n/N_t)^2}{(n/\sqrt{n})^2} = [1 + \frac{N_r^2}{\eta^2 n}]^{-1} \qquad (2.11)$$

At full output, i.e. $n = S_{mx}/\eta$, Eq.(2.11) gives DQE very close to unity. At the lower dynamic limit , i.e. $n = n_{min}$, DQE falls with increasing m, as the readout noise increases. However, under typical conditions (Fig.2.4) DQE remains above 0.3 even for a minimum detectable signal, so the array can behave as an almost-ideal electron detector in the direct-exposure mode.

2.3 INDIRECT EXPOSURE TO ELECTRONS

In indirectly exposed devices, the electrons are converted into photons at a transmission or reflection phosphor (Fig.2.5). These photons are then imaged onto the

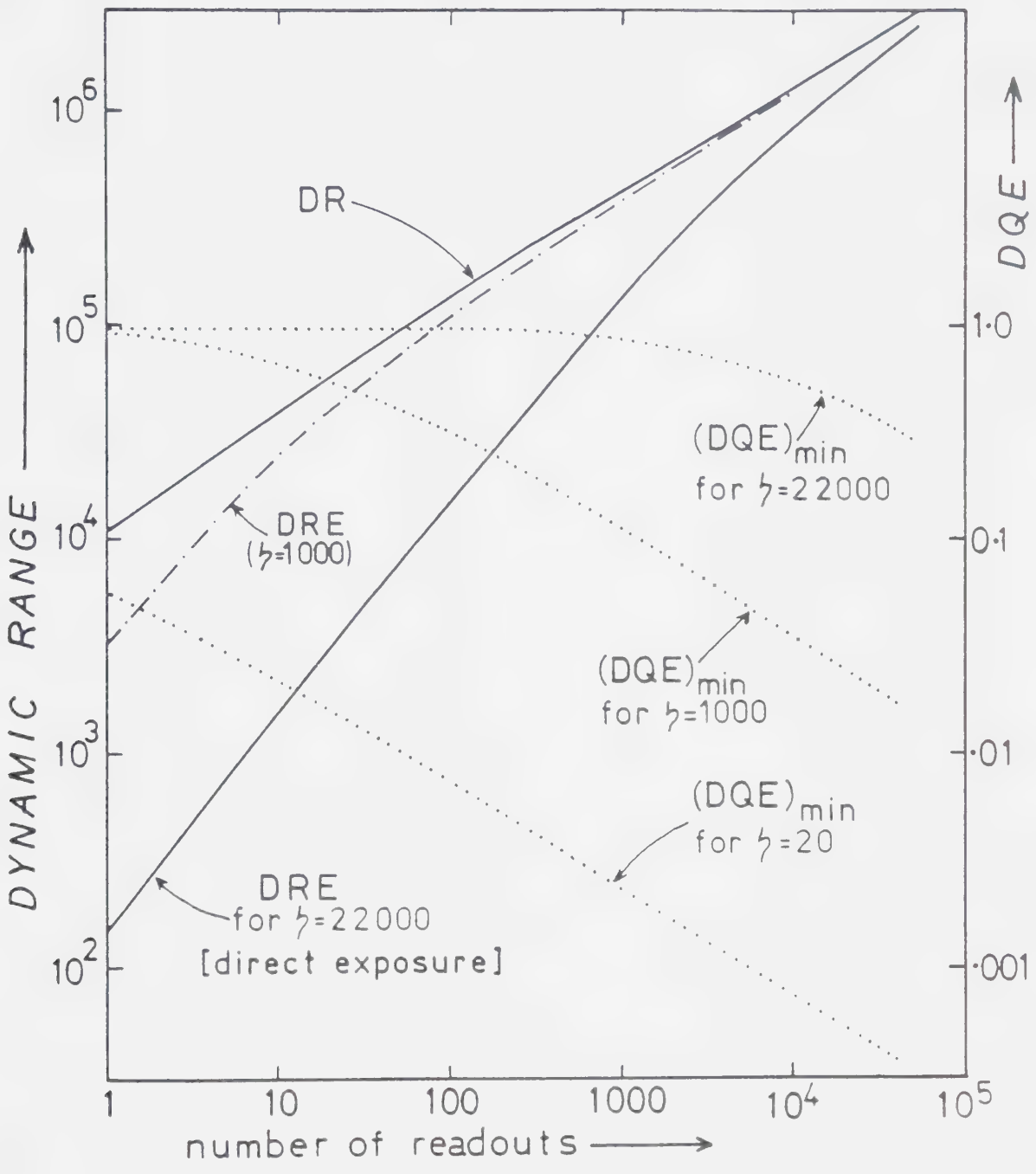

Figure 2.4 Dynamic range DR and DRE, Detection Quantum Efficiency at the lower dynamic limit DQE as a function of the number of readouts at -30 °C

array by means of a lens or coherent fibre optics. The use of fibre optics involves less light loss and is a relatively compact optical system, which requires no focussing and is relatively insensitive to mechanical vibrations. The use of lens optics has the advantage that the amount of transmitted light can be easily controlled by the use of an aperture stop. Both coupling optics mentioned above can be used to provide greater dispersion by incorporating image magnification.

Usually the energy resolution in indirect-exposure method will be reduced since an efficient phosphor (i.e. one that absorbs and converts all the electrons) will produce a broadened image point. However, the energy resolution in the indirect-exposure method can be comparable with the direct-exposure method, provided the phosphor is sufficiently thin or fine grained. This is true especially when magnifying optics are used between the phosphor and the array. There is also possibility of inserting a half-plane filter into the light-optical path in order to extend the dynamic range of the recorded electron intensities. More important, with existing commercial arrays having been designed to respond to visible photons, the indirect-exposure array is free from problems of radiation damage. The array is also protected from possible beam-induced hydrocarbon contamination and (if the factory-sealed protecting quartz or fibre-optic window is left in place) from dust particles, which could result in

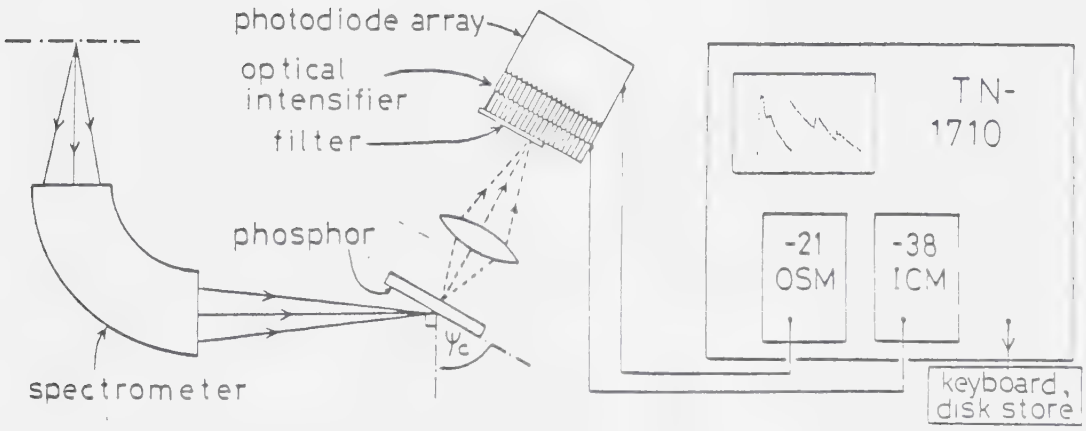

Figure 2.5 Schematic diagram of an EELS indirect-exposure parallel collection system

non-uniformities in the recorded output.

However, all these advantages are obtained at the expense of reduced efficiency because of the inevitable losses of efficiency at each interface in the system. With an efficient phosphor and fibre-optic coupling, the number of diode electrons (or electron hole-pair) produced at the array is of the order of 1000 per incident electron. This implies that the detector is therefore less sensitive, by a factor of at least 20, than in direct-exposure mode. Dynamic range DRE and Detection Quantum Efficiency DQE can be recalculated for the case of indirect exposure, using Eqs. (2.9), (2.10) and (2.11) but with a lower value of η. η=1000 and η=20 are for indirect exposure, using a P4 and NE102 screen, respectively. For these cases, the dynamic range DRE and the detection quantum efficiency DQE are also shown in Fig. 2.4. It is seen that the DQE is typically less than 0.3.

This value can be improved by using an image intensifier either integral with the target (Shuman 1981) or closely coupled to it (Egerton 1981 b, Johnson et al 1981 a b). Such devices improve the DQE by increasing the efficiency of light transfer and by multiplying the photon flux reaching the array. Since optical gains of the order of 10000 are possible, a gain of an order of magnitude may be possible in the DQE. One limitation of such an intensified detector is that the intensifier contributes additional variations in sensitivity along the array (Egerton 1981a).

Also, the optical intensifiers are easily damaged by overload and generate a certain amount of geometric distortion. Such distortion will result in the energy-loss scale being non-linear, particularly towards both ends of the field.

In summary, indirect-exposure systems present more design problems but allow control over the detector sensitivity and therefore an extension of dynamic range. However, the DQE is typically less than 0.3, a situation which can only be improved by using an optical intensifier between the phosphor and the array.

CHAPTER III

RADIATION DAMAGE TO THE PHOTODIODE ARRAY

3.1 INTRODUCTION

One of the more important questions associated with direct electron exposure relates to the possibility of radiation damage to the array by the electron beam. Obviously, under the bombardment of the high energy electrons not only the diodes but also the peripheral circuitry are at risk. Especially, the field-effect transistors (FET) used in the scanning circuitry adjacent to the photodiodes are easily damaged (Jones et al 1977). This may be the reason that early attempts to use a photodiode arrays directly in the beam often resulted in catastrophic failure. Fortunately, the associated readout circuitry can be protected by a metal mask placed close enough to the surface to prevent backscattered electrons reaching the transistors and thick enough to absorb not only the electrons but also the resulting high-energy X-rays (Jones et al 1980). With suitable masking, radiation damage to an array is greatly decreased but is still observed (Johnson 1977, Shuman 1981). Shuman reported that the thermal leakage current I_d of the diodes (when irradiation is removed) increased monotonically with total dose received during exposure of an array at room temperature, and was independent of the dose rate. Shuman also reported that after sufficient exposure, the radiation damage could be so

serious that the thermal leakage current saturated the output, rendering the device useless.

Fortunately, there appear to be a number of ways of dealing with the effect of irradiation damage. One way is to cool the array below room temperature, which greatly reduces thermal leakage current (Jones et al 1977 and 1980, Downing 1980). An alternative one is annealing, which is effective in restoring an array that has suffered irradiation damage (Snow et al 1967).

In the design or use of a directly exposed photodiode-array detection system for EELS, radiation damage is thus certainly one important factor to be considered. Also, the lifetime of the directly-exposed photodiode array needs to be defined in order to evaluate the degree of radiation damage.

In the following sections, a convenient definition of the operational lifetime of directly-exposed array is proposed, and measurements related to this quantity (for 100keV incident electrons) are presented and discussed.

3.2 EXPERIMENTAL

3.2.1 PHOTODIODE ARRAY

A Reticon 1024-element linear array was obtained from Reticon Corporation, 910 Benicia Avenue, Sunnyvale, California 94086. The aperture width of the array is 2.5 mm; the length is 26.01 mm. The detector elements are on 25.4 μm

spacing, which results in a density of 39.4 diode/mm. The arrays were operated using the RC-1024SA evaluation board, the video output being viewed on an oscilloscope. Only the central 1 mm of the 2.5 mm-wide array was utilized, the edges of the diodes and the peripheral MOS circuits being protected from the incident 100 keV electron beam by means of a rectangular mask (Fig. 3.1)

3.2.2 COOLING DEVICE

A refrigerator was used to cool an array and its control board in the range from room temperature to -20°C, in order to measure the leakage current as a function of temperature. The results are shown in Fig. 3.5. Because it took time to transfer the array from the refrigerator to the measurement area, the temperature of the array probably changed a little during transfer. This change was minimized by performing the transfer as quickly as possible, particularly at temperatures below -10°C.

An arrangement shown in Fig. 3.1 was used to cool an array during irradiation. The copper strip in contact with the backside of the array was connected by braiding to liquid N_2. The liquid N_2 level should be kept at the same level for a stable temperature. A photodiode array was exposed to the electron beam for more than one hour using this cooling arrangement; its leakage current was measured both before and after returning the photodiode array back to room temperature. Using the temperature dependence of

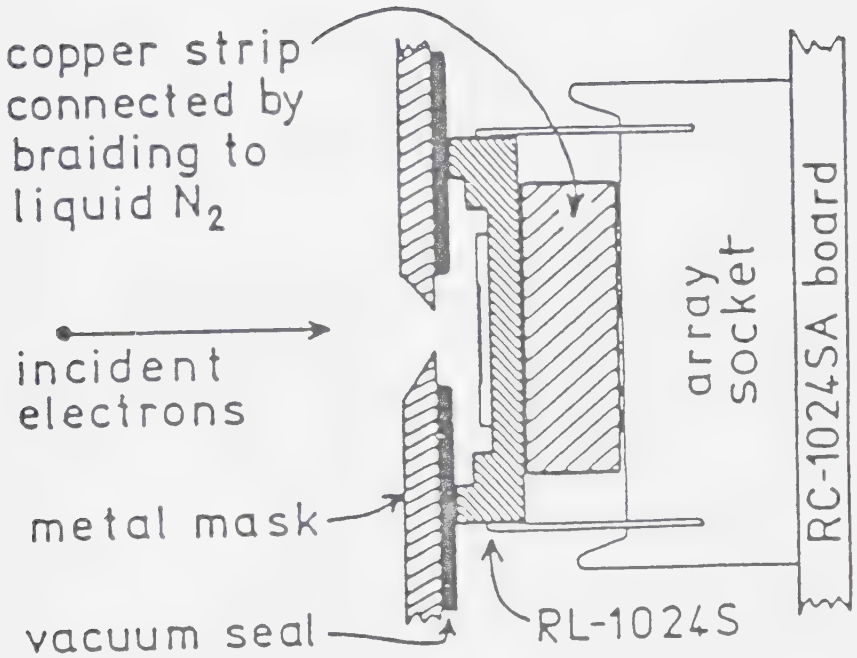

Figure 3.1 The arrangement used to cool an RL-1024S array during exposure to 100 keV electrons.

leakage current, shown in Fig. 3.5, the actual tempetature of the diodes (during irradiation) was estimated to be -30°C.

3.2.3 ANNEALING DEVICE

The device arranged for annealing is shown in Fig. 3.2. The array to be annealed was hung in the centre of a tube through which oxygen or argon (purity ≥ 99%) was passed. The tube was heated electrically. Its temperature was measured and controlled by a thermocouple and a commercial furnace-control unit (an indicating and controlling potentiometer, VERSA-TRONIK type R7161B).

3.3 PROPOSED DEFINITION OF THE OPERATIONAL LIFETIME OF A DIRECTLY-EXPOSED ARRAY

With the incident-beam intensity adjusted so that the video output amounted to half the maximum (saturation) value under the irradiation conditions in 3.2.1, the operational lifetime of a directly-exposed array was defined as the time taken for the output voltage to saturate, due to the increase in leakage current.

The lifetime, as defined, is a parameter which depends only on the diode array, and not on the integration time which we choose. If the integration time is increased by a factor of k, the incident-beam intensity has to be reduced by a factor of k in order to restore the output to half the maximum (saturation). Experiments (Downing 1980, Shuman

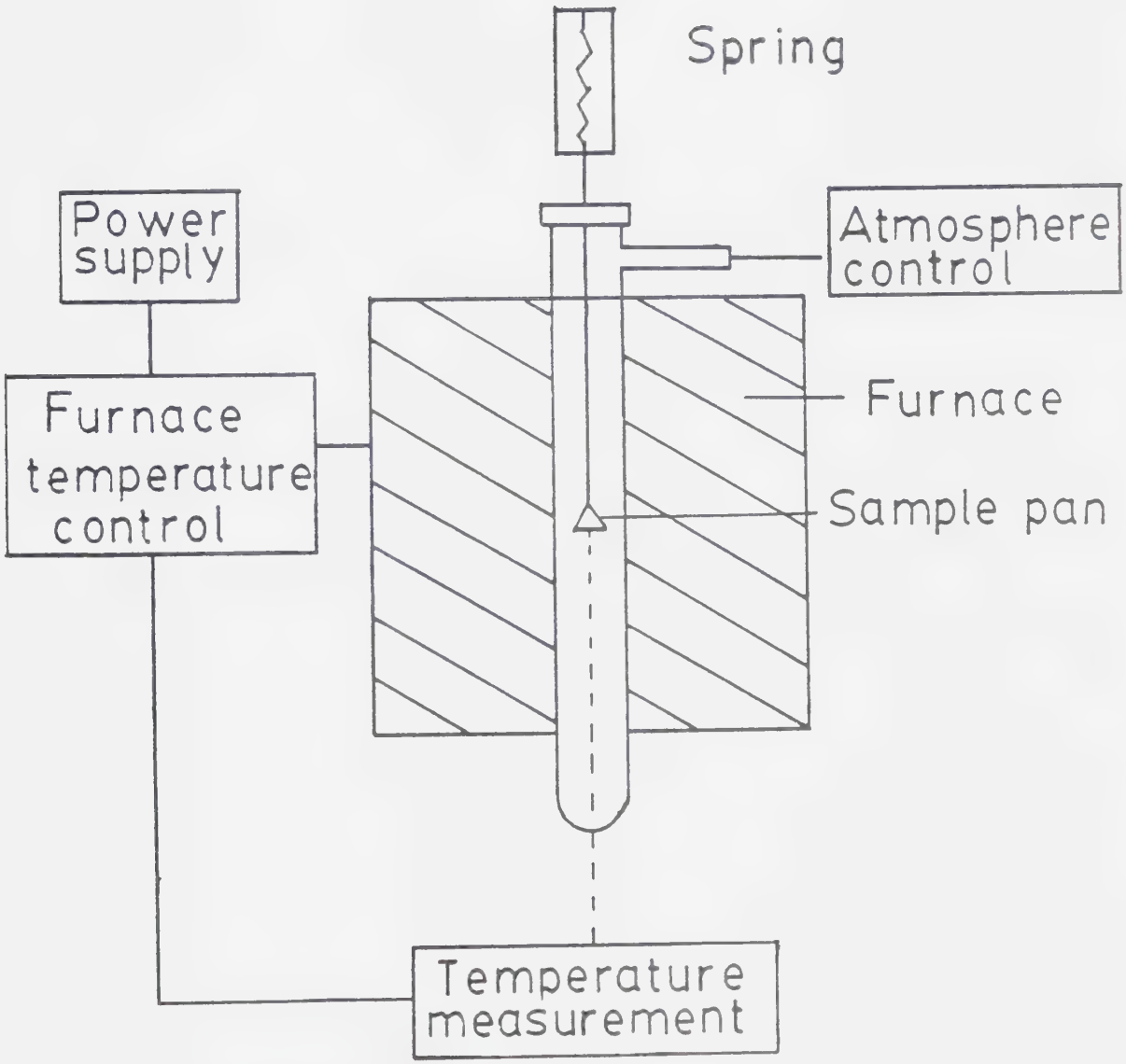

Figure 3.2 The arrangment used for annealing an array.

1981) have shown that the induced leakage current is roughly proportional to the electron-beam dose, which is proportional to the product of incident-beam intensity and exposure time. Therefore the increase in leakage current will be reduced by a factor of k after the same exposure time; but because the integration time is now k times longer than before, the total increase in leakage current will be the same as in the first case. This means that our definition of lifetime is independent of the value of k, i.e. that the lifetime is independent of the integration time.

3.4 RESULTS AND DISCUSSION

3.4.1 THE LIFETIME OF AN ARRAY AT ROOM TEMPERATURE

Figure 3.3 illustrates the observed behaviour during irradiation by 100 keV electrons at room temperature. An increase in leakage current is observable after only a few minutes, but if either the incident beam or the d.c. power to the array is turned off, the device "recovers" substantially, such that the permanently-induced leakage current is an order of magnitude smaller. Because of this recovery effect, operational lifetime at room temperature would be higher if an array were used intermittently, as opposed to being continuously irradiated. Assuming the excess leakage current to be roughly proportional to electron exposure (Downing 1980, Shuman 1981), the projected

lifetime can be estimated from Fig. 3.3 to be : (2.5/0.1)*10 = 250 minutes≃ 4 hrs. (2.5v is half of saturation voltage).

The above observations can be explained by the radiation-induced space-charge buildup in the SiO_2 passivating layer (Snow et al 1967). The upper part of Fig. 3.4 presents the cross section of a silicon diode before irradiation, where SiO_2 has the normal thickness of 3μm. During electron irradiation, the incoming electrons penetrate the SiO_2 barrier layer and enter the silicon substrate, where electron-hole pairs are generated. However, it is believed that electron-hole pairs are also generated in the SiO_2 passivating layer. The electrons within the SiO_2 layer and particularly within the region of impact ionization are quite mobile. These electrons can, therefore, participate in recombination events in the silicon beneath the SiO_2 layer. But the holes within the SiO_2 layer are not mobile. Thus, a positive charge will build up as electrons are removed from the oxide layer; consequently, the surface of the p-type silicon is inverted to n. As a result, the junction area is extended and an additional transition region of very small width is created as shown in the lower part of Fig. 3.4. Being electrically in parallel with the original junction, this additional narrow transition region can greatly increase the leakage current. Switching off power to the array, even if the electron beam is left on (Fig. 3.3), means that the electrical bias is removed. Thus electrons might be expected to drift back into the SiO_2

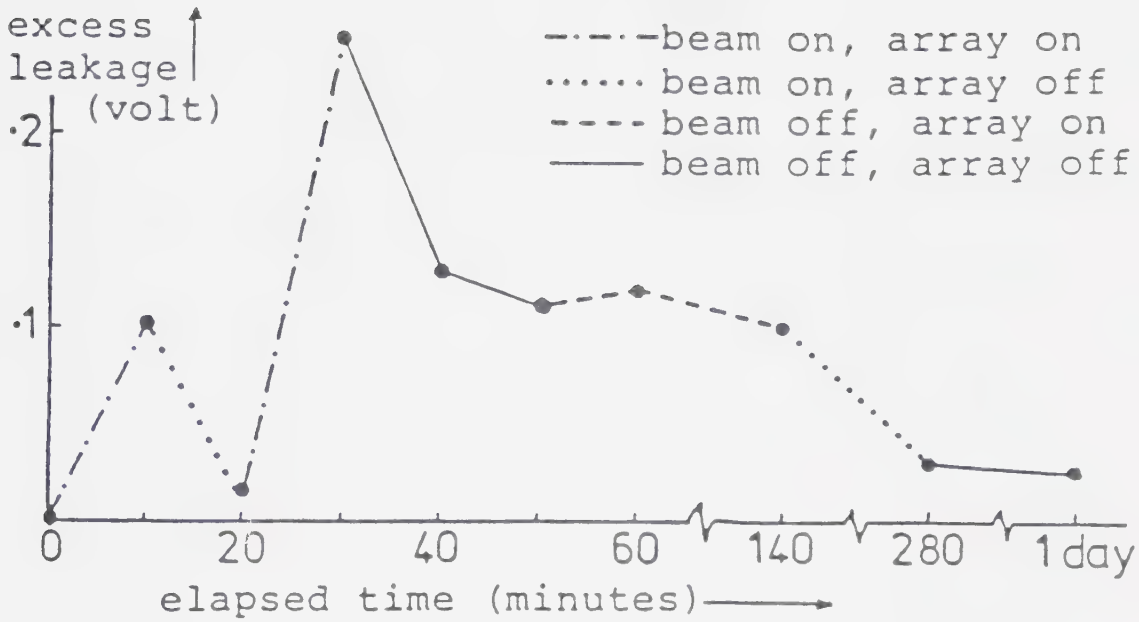

Figure 3.3 Increase in the leakage current of diodes in an RL-1024S array which was exposed to a 100 keV electron beam at 27 °C. The beam intensity corresponded to 50% saturation.

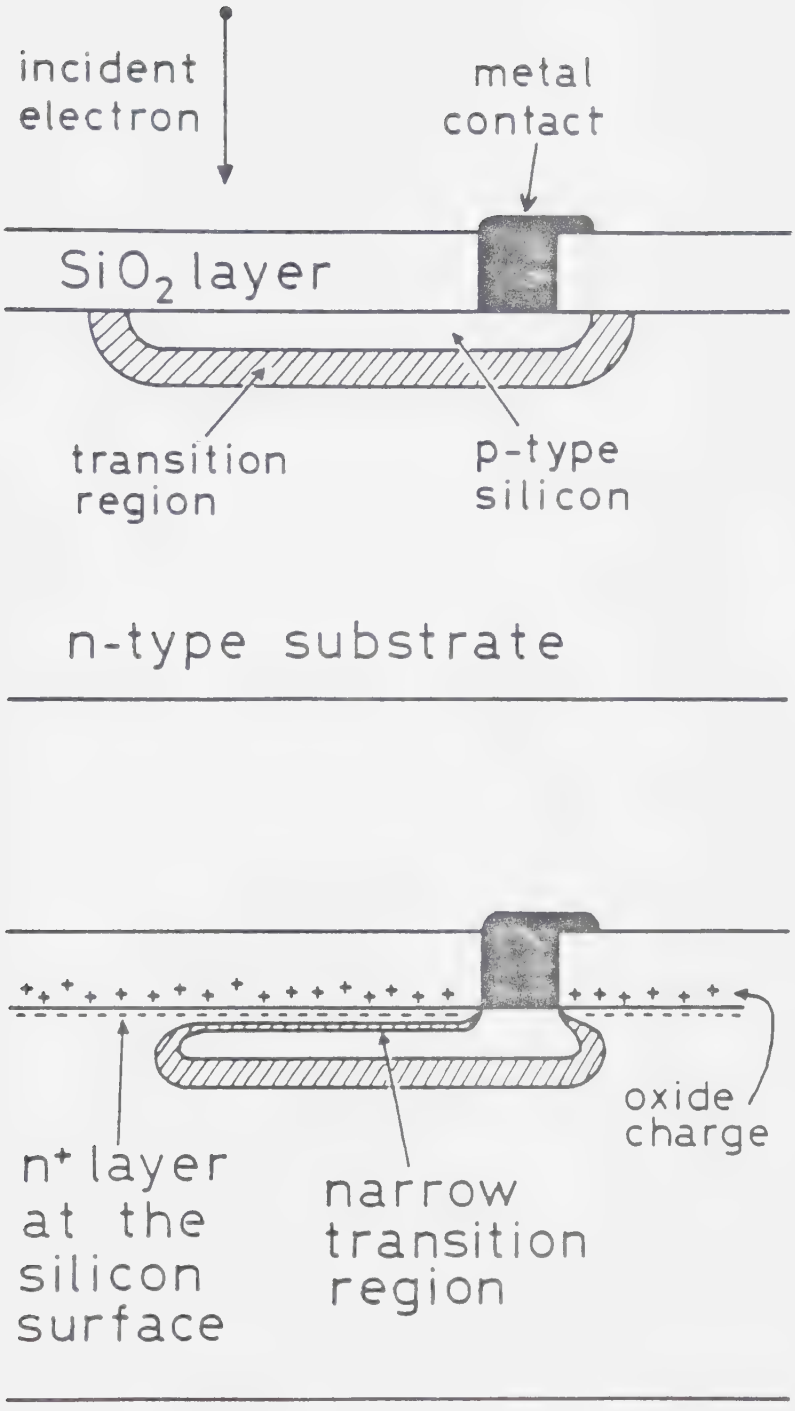

Figure 3.4 Cross section of a silicon diode before and after irradiation

passivating layer, neutralizing the space charge. Therefore a radiation-induced increase in leakage current I_d gradually disappears (i.e. the device "recovers").

3.4.2 EFFECT OF TEMPERATURE

While the lifetime of an array at room temperature is only 4 hrs. (3.4.1), a substantial improvement upon cooling the array would be expected. Figure 3.5 presents the temperature dependence of the excess leakage current after the array has suffered from radiation damage. This was measured by operating the array (and circuit board) at several temperatures. The results show that (like the normal thermal leakage current) the radiation-induced leakage current is strongly temperature dependent, decreasing by a factor of two for every 10 °C of cooling. This is because the number of charge carriers (electrons and holes) generated by thermal excitation decreases exponentially as temperature decreases (as described by Boltzmann's law). In addition, the generation of space charge by the incident beam might be expected to be a thermally activated process. To test the latter hypothesis, the simple arrangement shown in Fig. 3.1 was used to cool an array to about -30 °C during irradiation. At this temperature, leakage current remained unmeasurable after one hour of continuous irradiation ($\leq$ 2mV). Upon returning the device to room temperature, excess diode leakage in the irradiation region amounted to only 1% of saturated output (50mV). Since the lifetime of an array

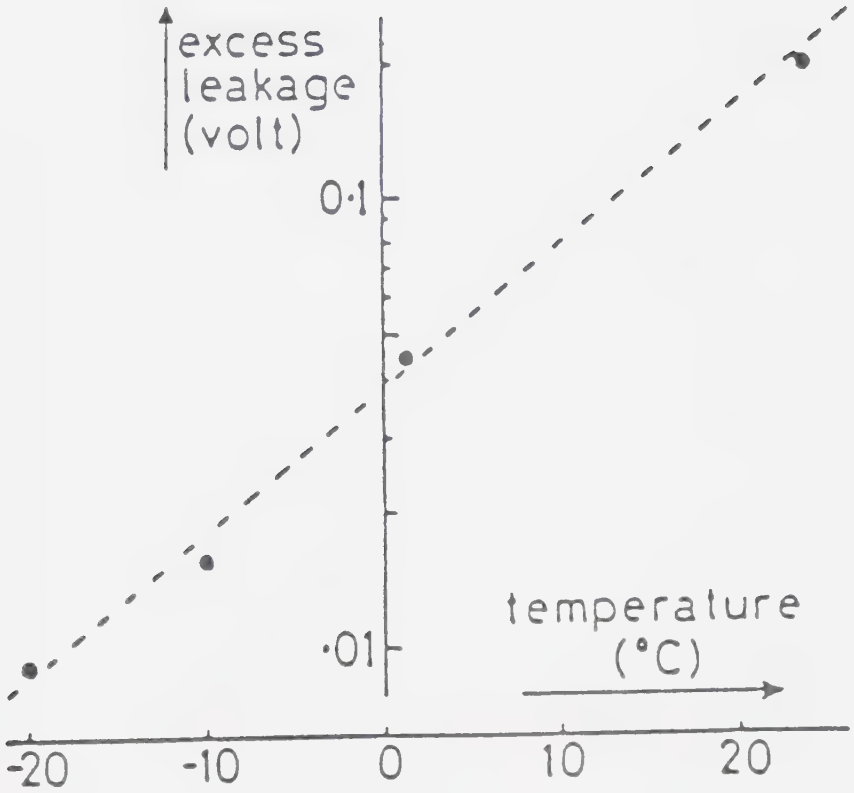

Figure 3.5 Temperature dependence of the radiation-induced leakage current, measured by operating the array (and circuit board) at several ambient temperatures.

at room temperature is 4 hrs. the leakage current would have been 50%*(1/4) =12.5% of saturated output (625mV) after one hour of continuous irradiation at room temperature. This confirms that the rate of space-charge buildup was substantially reduced by cooling.

Based on these measurements, the commercially-available arrays are estimated to have a useful lifetime : 1 hour*(2500mV/2mV) = 1250 hrs. if operated at or below -30 °C (Egerton and Cheng 1982). In support of this, Jones et al (1982)have reported no significant degradation of an array irradiated at -40 °C by 100 keV electrons, provided the scanning circuitry adjacent to the photodiode is masked from the beam and the incident current density is kept bolow 10^{-8} A/m^2.

As to the cooling device, the arrangement shown in Fig. 3.1 is simple but not convenient (the liquid nitrogen level had to be topped up frequently). An alternative method is to use a two- or three-stage thermoelectric (Peltier-effect) device, in which a temperature below -30 °C to -70 °C can be achieved (see 4.2.2).

3.4.3 ANNEALING OF AN ARRAY

Thermal annealing was performed using the device shown in Fig. 3.2. It was found that thermal annealing for a few minutes (1 to 3 minutes) at 300 °C reduced the leakage current by 50%, and 30 to 60 minutes at 300 °C reduced the leakage current by 95%. This implies that thermal annealing

will be effective in restoring an array which has suffered irradiation damage, and thus will extend the lifetime of the array.

This result is in agreement with the result of annealing CCD 's (Roberts et al 1982). The annealing mechanism is that under thermal conditions electrons are injected from the silicon into the SiO_2 passivating layer, hence reducing the positive space charge (Snow et al 1967).

3.5 CONCLUSIONS

Radiation damage is a major drawback of directly-exposed photodiode arrays. However operation of an array at low temperature (-30 °C) greatly extends its lifetime, and is thus very encouraging. An even lower temperature would be expected to further extend the lifetime. Also, various forms of annealing could restore an array which has suffered irradiation damage. Probably an ultimate solution is the production of future devices immune to electron-irradiation damage. The possibilities include optimization of device geometry, minimizing the oxide thickness and use of an alternative dielectric material at the surface (Killiany 1978).

CHAPTER IV

SOME DESIGNS FOR A PHOTODIODE-ARRAY DETECTION SYSTEM

In this chapter, two designs for a SSD array parallel detection system will be presented. One is the design of a post-spectrometer lens system in order to increase the energy resolution of the spectrum, which is important for parallel recording. Another is a serial-parallel combination detection system designed to record the spectrum over a range which includes zero and low-energy losses, as well as energy losses as high as 2000 eV or 4000 eV.

4.1 DESIGNS FOR A POST-SPECTROMETER LENS SYSTEM

4.1.1 INTRODUCTION

The need for a post-spectrometer lens system is based on the requirement for good energy resolution in the spectrum. Usually in serial detection one is able to choose the width of the detector slit as a compromise between energy resolution and signal/noise ratio. However, no such compromise is involved in the case of a parallel detection system. Hence a parallel detection system should be designed to give as good energy resolution as possible, within the limits in energy spread imposed by the electron source.

Although the energy dispersion in EELS can be obtained by applying to the transmitted beam a transverse magnetic or

electric field or a combination of the two, the type of spectrometer considered here will be the magnetic spectrometer which is more popular for the following reasons. First, a magnetic spectrometer is simple and inexpensive to construct, and high voltages are not involved in its operation. Also, its spectrum is formed along a straight line, allowing a parallel detector slit or a linear detector array to be employed. In addition, the dispersive power is approximately constant up to high energy loss, giving a linear energy scale.

The basic design is shown in Fig. 4.1; the magnetic field bends the electron beam through an angle ϕ with a radius of curvature R and has a focussing action on electrons travelling in the x-z plane. Focussing in the y-direction is achieved by tilting the entrance and exit edges of the polepieces through angle ϵ_1 and ϵ_2. For ϕ = 90°, equal focussing in the x and y directions occurs when $\epsilon_1 = \epsilon_2 = 26.5°$, giving a single (point) focus at a distance V = 2R from the exit face for a point object located a distance u = 2R from the entrance.

The energy dispersive power, D, for such a symmetric, double-focussing spectrometer is given by

$$D = \frac{\Delta X}{\Delta E} = \frac{4R}{E_i} \left[\frac{E_i + E_r}{E_i + 2E_r}\right] \qquad (4.1)$$

where E_r is the electron rest energy (Egerton 1980). For typical values: E_r = 511 keV, E_i = 80 keV and R = 20 cm, D is about 5.4 μm/eV. Although some spectrometers depart from

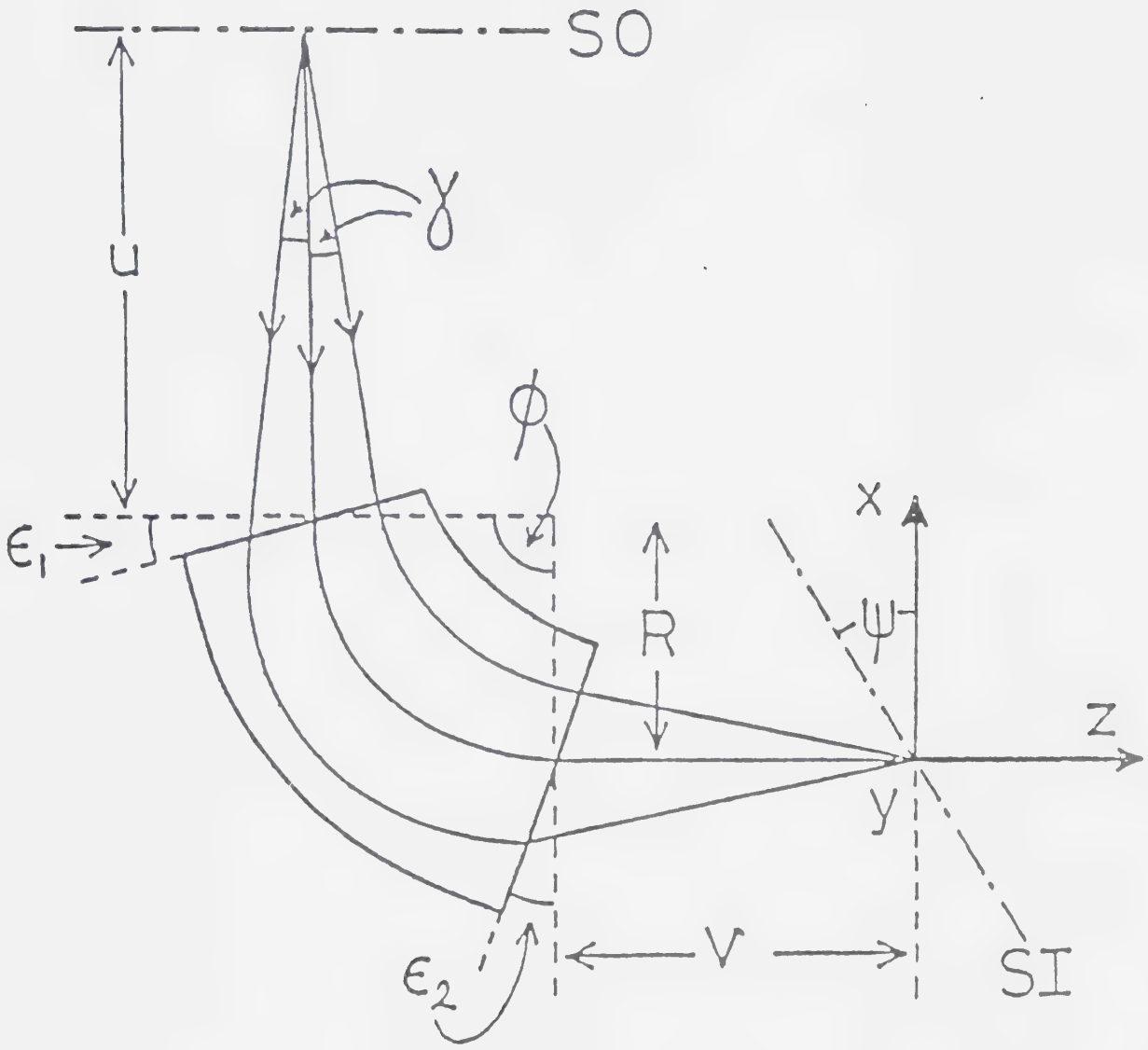

α maximum scattering angle contributing to the energy-loss spectrum (radians)

ψ tilt of spectrometer plane-of-focus, relative to the x-axis (radians)

γ maximum spectrometer entrance angle, relative to the central beam (radians)

ϕ bend angle of electron beam in spectrometer (radians).

Figure 4.1 General optics of a magnetic spectrometer.

this symmetric geometry, their performance is not greatly affected. For example, the spectrometer used in our laboratory, connected to a JEM100B, gives a D value of 5.1 μm/eV at $\epsilon_1 = 20°$ and $\epsilon_2 = 30°$. Therefore it might be reasonable to say that most magnetic spectrometers give a dispersive power (for 80 or 100 keV electrons) of 5 μm/eV or less.

However, the spacing between active diodes in a linear photodiode array (e.g. 1024 channel Reticon array) is typically 25 μm. In addition, 80 keV incident electrons will penetrate by about 40 μm and thus spread laterally by about up to 30 μm (Cosslett and Thomas 1964), causing so-called "cross talk" between diodes. As a result of the finite channel width of the diode and the "cross talk" between the diodes, the spatial resolution of an array for the detection of 80 or 100 keV electrons will be not better than about 50 μm. Therefore, when such a linear photodiode array is placed in the focus plane of a magnetic spectrometer having a D value of 5 μm/eV, the energy resolution is expected to be

$$\Delta E = \Delta X/D \simeq 50\mu m/(5\mu m/eV) = 10 \text{ eV}$$

This value is large compared with the spread of electron energy caused by the thermal spread of the source and instabilities of the high tension supply, which is only about 2 eV (Hall 1966).

The simplest way of increasing the energy resolution is to tilt the array away from normal incidence (Egerton 1981). An alternative way is to add an electron lens to image the

spectrum from the focus plane of the spectrometer to an image plane where a detector is placed. In this way the resolution can easily be increased by a factor of 4 or 5, reaching about 2 eV. However, the usual type of axially-symmetric magnetic lens has the property of rotating the image, resulting in additional complexity to the system. This problem can be solved by employing a double, symmetric lens, or by a quadrupole lens, or by special lens designs (Mulvey 1982).

Here are presented designs for three rotation-free lens systems: a double symmetric magnetic lens, a single magnetic quadrupole lens and a quadrupole doublet lens. One of them, the double symmetric magnetic lens, has been manufactured and used in our work.

4.1.2 THE DESIGN OF A DOUBLE SYMMETRIC ELECTRON MAGNETIC LENS SYSTEM

It is well established (Hall 1966) that an approximate expression for the focal length of a magnetic lens, f, if it is long compaired with the axial extent of the field, ℓ, is given by:

$$\frac{1}{f} = \frac{e}{8mC^2\phi} \int_0^{\ell} H_z^2 \, dz \qquad (4.2)$$

and the rotation angle of the image, θ, is (without approximation):

$$\theta = \left(\frac{e}{8mC^2\phi}\right)^{\frac{1}{2}} \int_0^{\ell} H_z \, dZ \qquad (4.3)$$

where

e is the charge of the electron,

m is the rest mass of the electron,

c is the velocity of light,

ϕ is the accelerating voltage,

H(z) is the magnetic field on the axis of a round magnetic lens.

Introducing numerical values for the constants in these equations, we have

$$\frac{1}{f} = \frac{0.022}{V} \int_0^{\ell} H_z^{\,2} \, dZ \quad cm^{-1} \qquad (4.4)$$

and

$$\theta = \frac{0.149}{\sqrt{V}} \int_0^{\ell} H_z \, dZ \quad \text{radians} \qquad (4.5)$$

where V is the accelerating voltage expressed in volts.

For iron-free lenses made of coils with radius R, H(z) can be calculated, to a good approximation, as

$$H_z = \frac{2\pi R^2}{(R^2+z^2)^{\frac{1}{2}}} \frac{NI}{10} \qquad (4.6)$$

where NI is the ampere-turns in the coil. If the coil is enclosed in magnetic materical, the field H(z) is increased

and the width of the fringing field reduced as shown in Fig. 4.2. In this case H(z) can be expressed, with approximation, by (Ximen 1979)

$$H_z = H_o \, \mathrm{sech}^2(2.63z/2R) \tag{4.7}$$

Substituting for H(z) in Eq.(4.4) from Eq.(4.7), and noticing that H(z) satisfies the following relation:

$$\int_{-\infty}^{\infty} H_z dz = \frac{4\pi NI}{10} \tag{4.8}$$

we get (Ximen 1979)

$$f = G\frac{V}{(NI)^2} R, \quad G = 64 \, \frac{(\text{Ampere-turns})^2}{\text{Volts}} \tag{4.9}$$

It is seen from Eq.(4.5) that if a pair of symmetric lenses, (having the same geometry and having the same amount of current but in opposite directions flowing through the coils) are used, a rotation-free image is obtained. For such combination lens system (Fig. 4.3), the following lens equations should be satisfied:

$$\frac{1}{a} + \frac{1}{b} = \frac{1}{f} \tag{4.10}$$

$$\frac{1}{f} = \frac{1}{f_1} + \frac{1}{f_2} - \frac{S}{f_1 f_2} \tag{4.11}$$

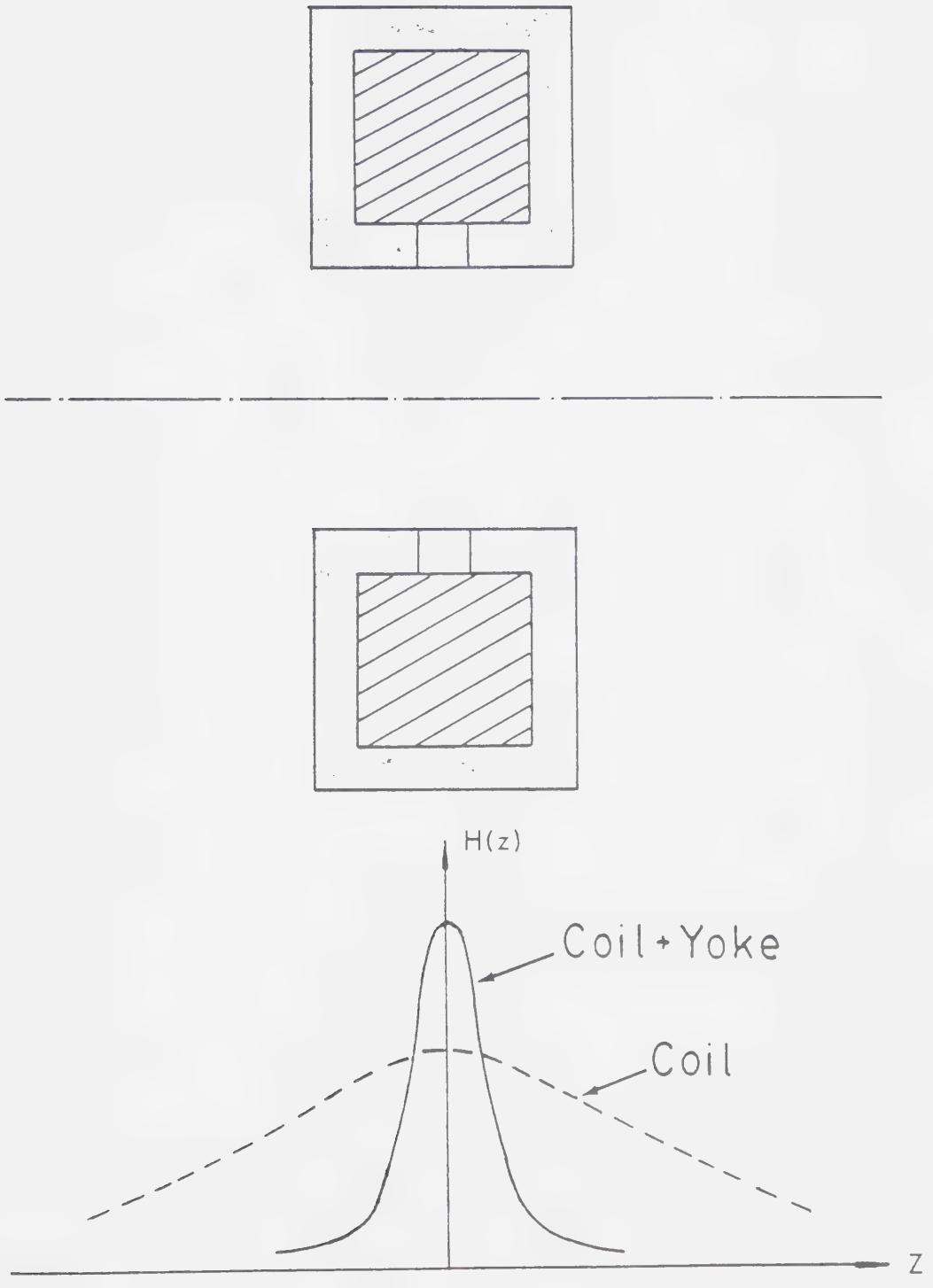

Figure 4.2 Magnetic field strength distributions for an iron-free lens, and for coils with an outer magnetic casing.

where

a is the object distance,

b is the image distance,

s is the separation of the lenses,

f, f_1 and f_2 are the focal length of the system, and of the two lenses, respectively. Thus, when a, b and s are fixed according to the required magnification and the distance between the object (the focus plane of the spectrometer) and the image (where a detector is placed), f_1 and f_2 ($f_1 = f_2$) can be calculated from Eqs.(4.10) and (4.11). Then, substituting for f_1 or f_2 in Eq.(4.9), the number of ampere-turns, NI, for each lens can be obtained.

In this design, the magnification required is 4 (4.1.1). We choose:

$$a = 43 \text{ mm}$$

$$b = 173 \text{ mm}$$

$$s = 34 \text{ mm}$$

so we have

$$f \simeq 35 \text{ mm}$$

$$f_1 = f_2 = 35 \text{ mm}$$

and

$$(NI)_1 = (NI)_2 = 1943 \text{ Ampere-turns}$$

The cross section of the lens system designed is shown in Fig. 4.3. The calculation of the power needed for this lens system is straightforward. When the diameter of the wire is chosen as 0.85 mm, the required power is 22 Watts; thus a Lambda LDS-Y-02 power supply is employed.

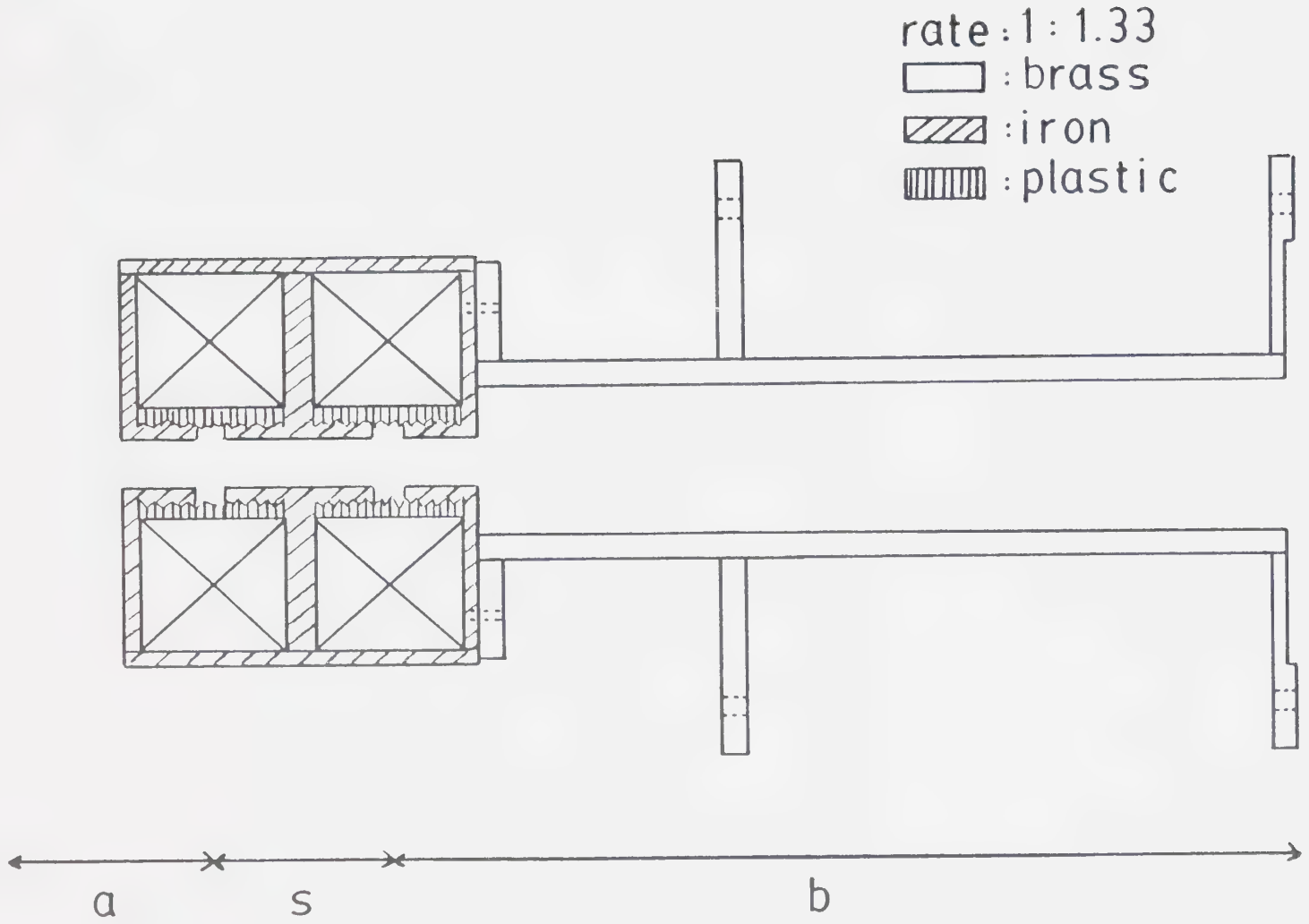

Figure 4.3 Cross section of a double, symmetric magnetic lens system

Figure 4.4 is the photograph of the rotation-free electron magnetic lens system built by the workshop in the Department of Physics, University of Alberta, according to the design given above. The oscilloscope trace of the spectrum of Al obtained with the incorporation of the above post-spectrometer lens system and a SSD array parallel detector is shown in Fig. 4.5. The dispersive power, calculated from the separation of the zero-loss peak and the plasmon peaks shown in Fig. 4.5, is 25 μm/eV, i.e. enlarged by a factor of about 5, This is in satisfactory agreement with the original design.

4.1.3 THE DESIGN OF A SINGLE MAGNETIC QUADRUPOLE LENS

In a quadrupole system electrons incident in the two planes perpendicular to each other will follow quite different paths. Electrons will be convergent in one plane, while divergent in the perpendicular direction, as shown in Fig. 4.6. If the convergent (x-z) plane is chosen to be the spectrometer bend plane, convergence in two directions is not strictly necessary for a Reticon 1024 photodiode array having an aperture width of 2.5 mm, provided the divergence angle is not too large (as will be seen later).

For short quadrupole lenses, the bell-shaped model can be used for analysis (Hawkes 1970). In this model the function defining the shape of the quadrupole potential is given by

Figure 4.4 Photograph of the rotation-free lens system made of a double symmetric magnetic lens

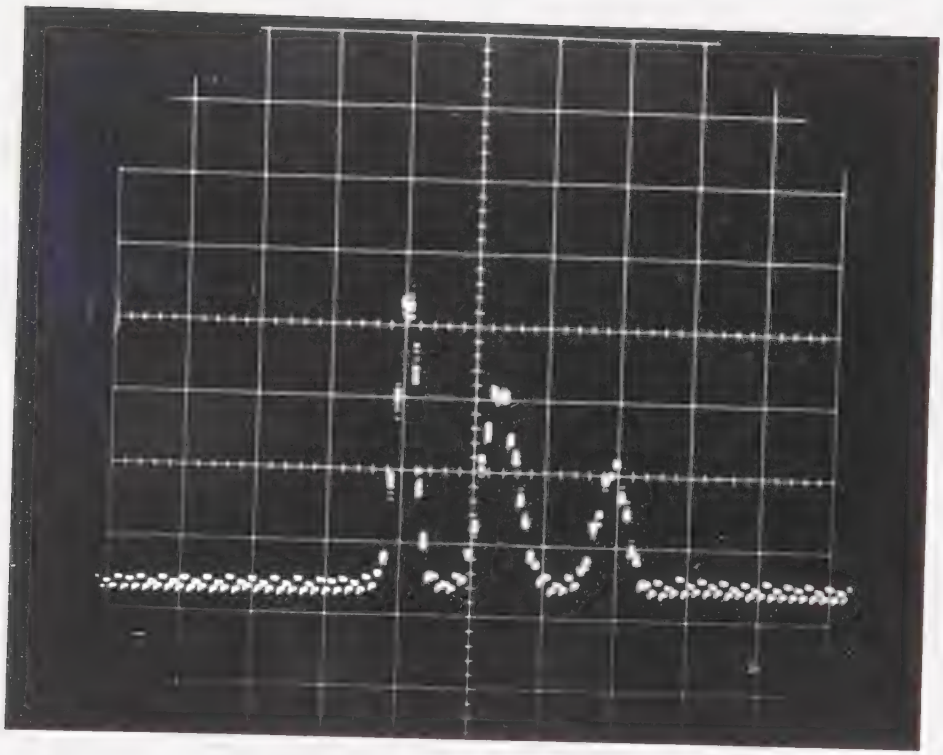

Figure 4.5 Oscilloscope tracing of the spectrum of Al, obtained with the incorporation of the designed post-spectrometer lens and a SSD array detector

$$K(z) = \frac{1}{\{1 + (z/\ell)^2\}^2} \qquad (4.12)$$

and the field- strength parameter, β, is given by

$$\beta^2 = \mu_o \eta \ \frac{NI}{r^2 V^{\frac{1}{2}}} \left(1 - \frac{r^2}{3\ell^2}\right) \qquad (4.13)$$

where

ℓ denotes the effective length of the quadrupole,

r denotes the bore radius of the quadrupoles (Hardy 1977),

NI is the amp-turns circulating in the coil around each pole piece,

μ_o and η are constants ($\mu_o \eta = 0.3726$).

For a short lens, in which $r \simeq \ell$, $1 - (r^2/(3\ell^2)) = 0.67$.

If we let

$$\omega_x^2 = 1 + \beta^2 \ell^2 \qquad \omega_y^2 = 1 - \beta^2 \ell^2 \qquad (4.14)$$

then the asymptotic cardinal elements are given by

$$\frac{f}{\ell} = - \frac{\omega x}{\sin \pi \omega_x} \qquad \frac{(zF)_i}{\ell} = - \frac{(zF)_o}{\ell} = \omega_x \cot \pi \omega_x$$

$$\frac{g}{\ell} = - \frac{\omega_y}{\sin \pi \omega_y} \qquad \frac{(zG)_i}{\ell} = \frac{(zG)_o}{-\ell} = \omega_y \cot \pi \omega_y \qquad (4.15)$$

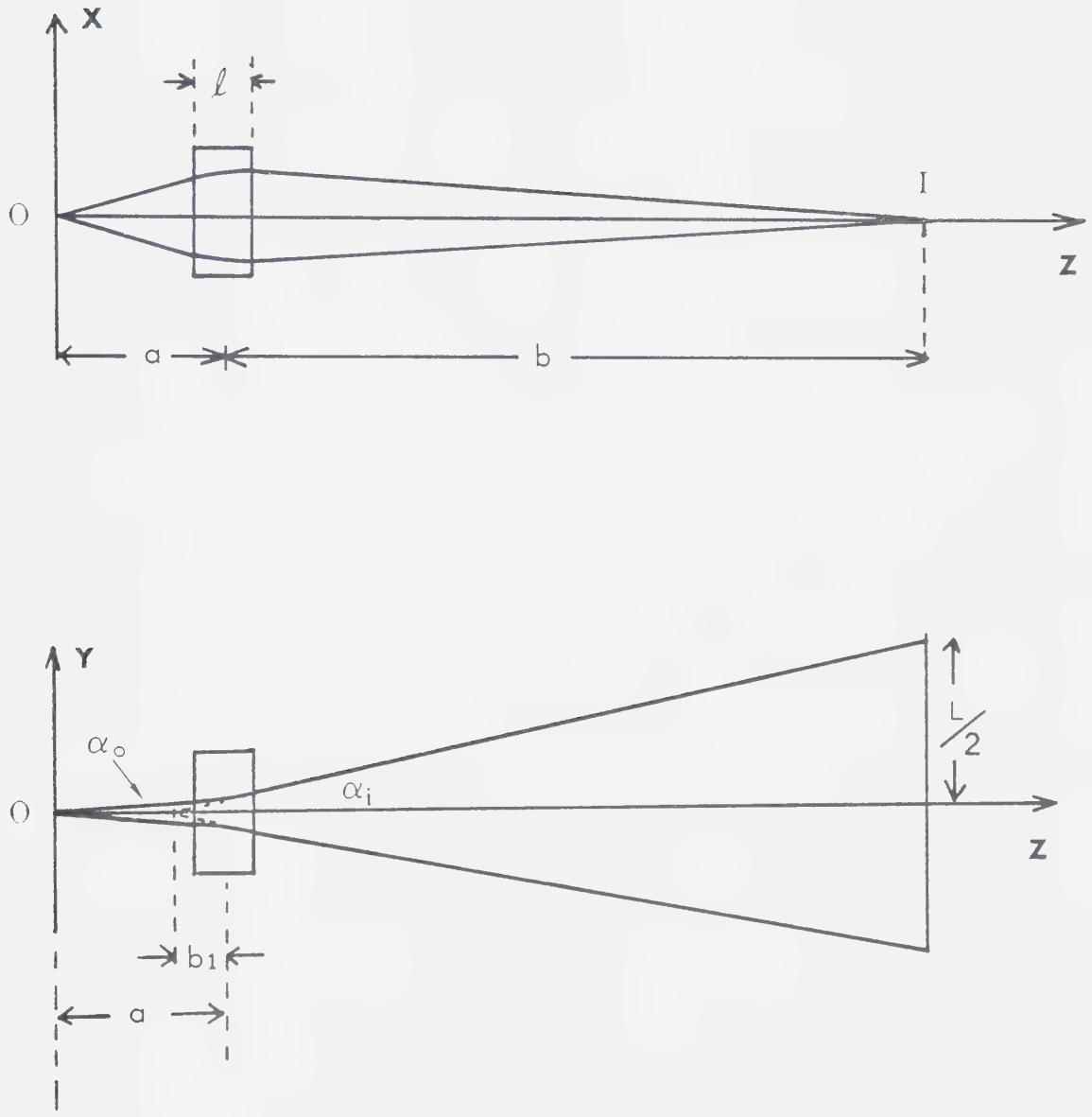

Figure 4.6 Particle trajectories in two planes of a quadrupole lens

where

f denotes the asymptotic focal length of the quadrupole in the x-z plane,

g denotes the asymptotic focal length of a quadrupole in the y-z plane,

$(Zf)_o$, $(Zf)_i$ are positions of the asymptotic object (o) and image (i) foci the quadrupole in the x-z plane.

$(Zg)_o$, $(Zg)_i$ are positions of the asymptotic object (o) and image (i) foci of the quadrupole in the y-z plane.

Assuming the distance from the object to the image (Fig. 4.6) is 100 mm, and the magnification in the converging (x-z) plane is 4, then

$$a = 20 \text{ mm}$$

$$b = 80 \text{ mm}$$

and according to lens equations the focal length of the quadrupole in the converging (x-z) plane is

$$f = 16 \text{ mm}$$

Let $f/\ell = 2$, then

$$\ell = 8 \text{ mm}$$

Thus, from Eqs.(4.14) and (4.15), we have

$$\beta = 0.85 \text{ mm}^{-1}$$

For 100 keV electrons, i.e. $V = 10^5$ volts, the number of ampere-turns, NI, can be calculated by subsituting for β and V in Eq.(4.13), giving:

$$NI = \frac{\beta^2 r^2}{0.67 \cdot \mu_o \eta} = 590 \text{ Ampere-turns}$$

This result shows that a magnetic quadrupole lens has a small power requirement, in comparison with an axially symmetric magnetic lens(4.1.2).

Now let us calculate the divergence width formed in the image (i.e. photodiode array) plane.

The focal length of the quadrupole in the devergent (y-z) plane can be calculated by using Eqs.(4.14) and (4.15); we have

$$g = -0.78 \text{ mm}$$

Since the object distance is still

$$a = 20 \text{ mm},$$

the image distance b_1 in the diverging (y-z) plane (Fig. 4.6) calculated using the lens equation is

$$b_1 \simeq -5.6 \text{ mm}$$

The angular magnification is equal to the inverse of the lateral magnification when α's are small; thus

$$\alpha_i/\alpha_o \simeq a/b_1 = -3.5$$

The divergence width in the detector plane (x-y) is therefore

$$\begin{aligned} L &= 2\cdot\alpha_i\ (b + b_1) \\ &= 2\cdot\alpha_o\ \left|\frac{a}{b_1}\right|\cdot(b+|b_1|) \end{aligned} \tag{4.16}$$

Usually, the angle α_o is determined by an aperture in the post-specimen lens or in the spectrometer. For α_o values of 5 mrad and 10 mrad, which are typical values in EELS, L will

be, according to Eq. (4.16), 3 mm and 6 mm respectively. This means that only 83% (for α_o = 5 mrad) or 41% (for α_o = 10 mrad) of the electrons forming the spectrum will be collected by the photodiode array having aperture width of 2.5 mm. The former ratio is still satisfactory but certainly not the latter. This situation can be greatly improved if a quadrupole doublet is used.

4.1.4 THE DESIGN OF A QUADRUPOLE DOUBLET LENS

In order to obtain an optical system that is convergent in all directions, two crossed quadrupoles, Q_1 and Q_2 are combined so that the convergent plane C of Q_1 coincides with the divergent plane D of Q_2; this yields a quadrupole doublet. Figure 4.7 shows the particle trajectories in two planes of a quadrupole doublet, where the x-z plane is referred to as the converging plane (last lens converging) while the y-z plane the diverging plane.

The field strength parameters β_1 and β_2 are given by the following relation:

$$\beta^2 = \mu_o \eta \frac{NI}{r^2 \sqrt{V}} \qquad (4.17)$$

The number of ampere-turns can be calculated by a graphical procedure (Enge 1959) illustrated as follows.
Let the magnification of the system be 4 and the distance between object and image (Fig. 4.7) be 100 mm, i.e.

$$a + b + 2\ell + s = 100 \text{ mm},$$

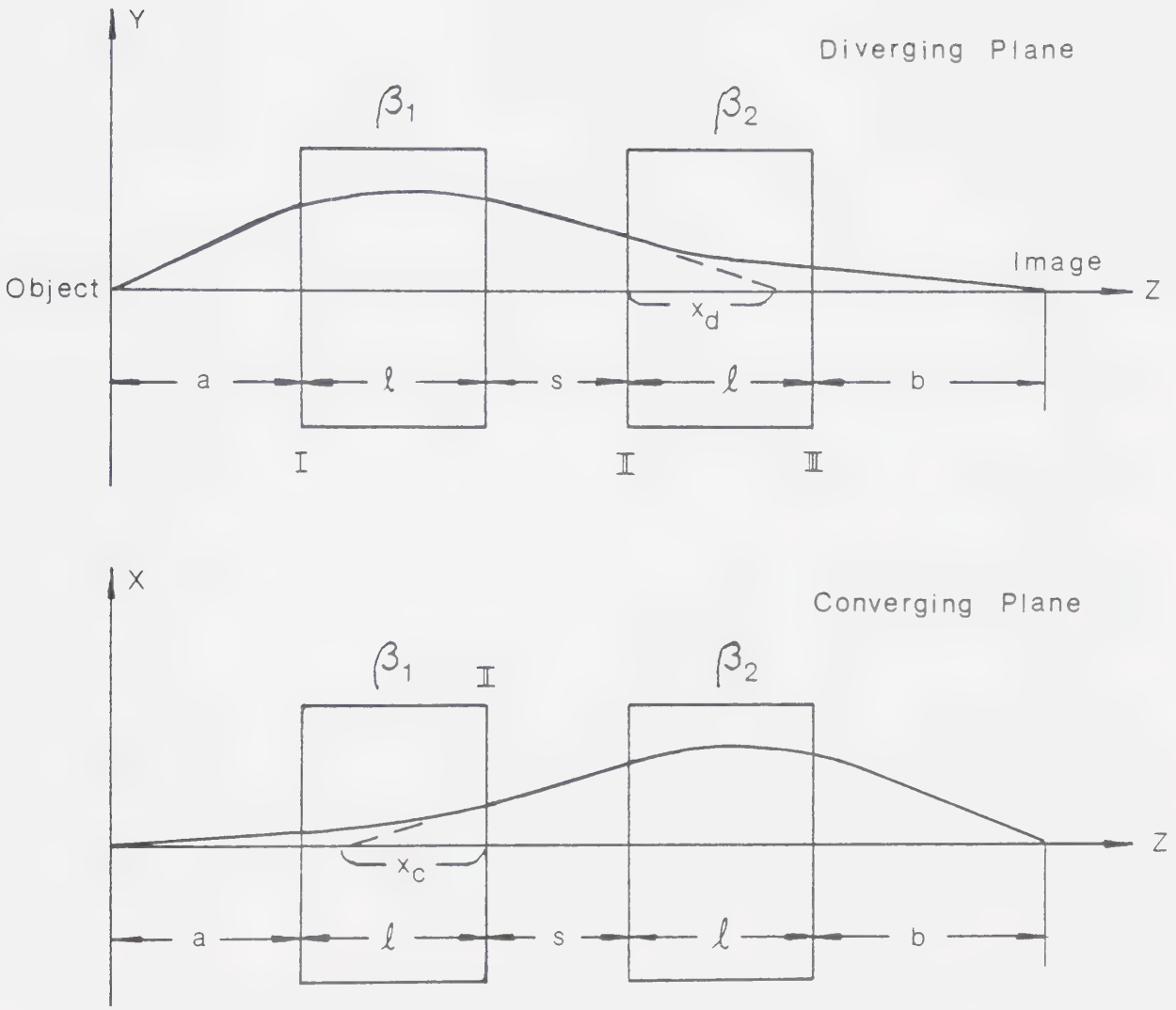

Figure 4.7 Particle trajectories in two planes of a quadrupole lens pair

and

$$\ell = s$$

$$a/\ell = 4$$

then from Fig. 4.8 we find

$$b/\ell \simeq 7.5$$

Thus we have $\ell \simeq 6.9$ mm With these values, the field strengh parameters β_1 and β_2 can be found from Fig. 4.9 (where k is equal to our β), i.e.

$$(\beta_1 \ell)^2 \simeq 0.57$$

$$(\beta_2 \ell)^2 \simeq 0.48$$

For 100 keV electrons, that is

$$V = 10^5 \text{ Volts}$$

and quadrupoles having

$$r = 0.69 \text{ mm}$$

The values of NI can be obtained from Eq.(4.17). They are:

$$(NI)_1 \simeq 483 \text{ Ampere-turns}$$

$$(NI)_2 \simeq 407 \text{ Ampere-turns}$$

It is seen that a quadrupole doublet needs less total number of ampere-turns and probably a lower power requirement than a double symmetric magnetic lens.

4.2 A SERIAL-PARALLEL COMBINATION DETECTING SYSTEM

4.2.1 INTRODUCTION

It has been mentioned in Chapter 1 that one basic requirement for detectors in EELS is to have a wide dynamic range; and usually a dynamic range $\geq 10^5$ is necessary for

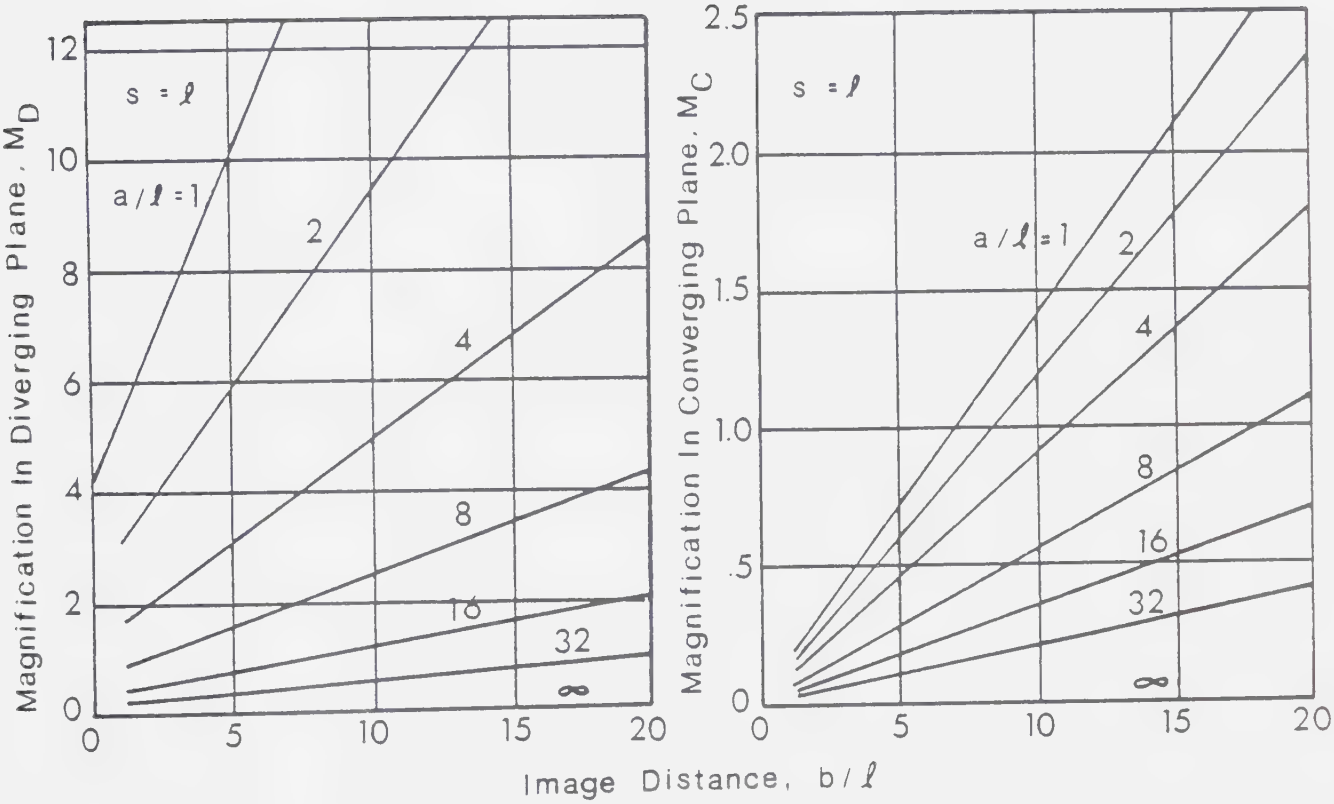

Figure 4.8 Magnification factors *vs.* object and image distances for a quadrupole lens pair of separation s = ℓ.

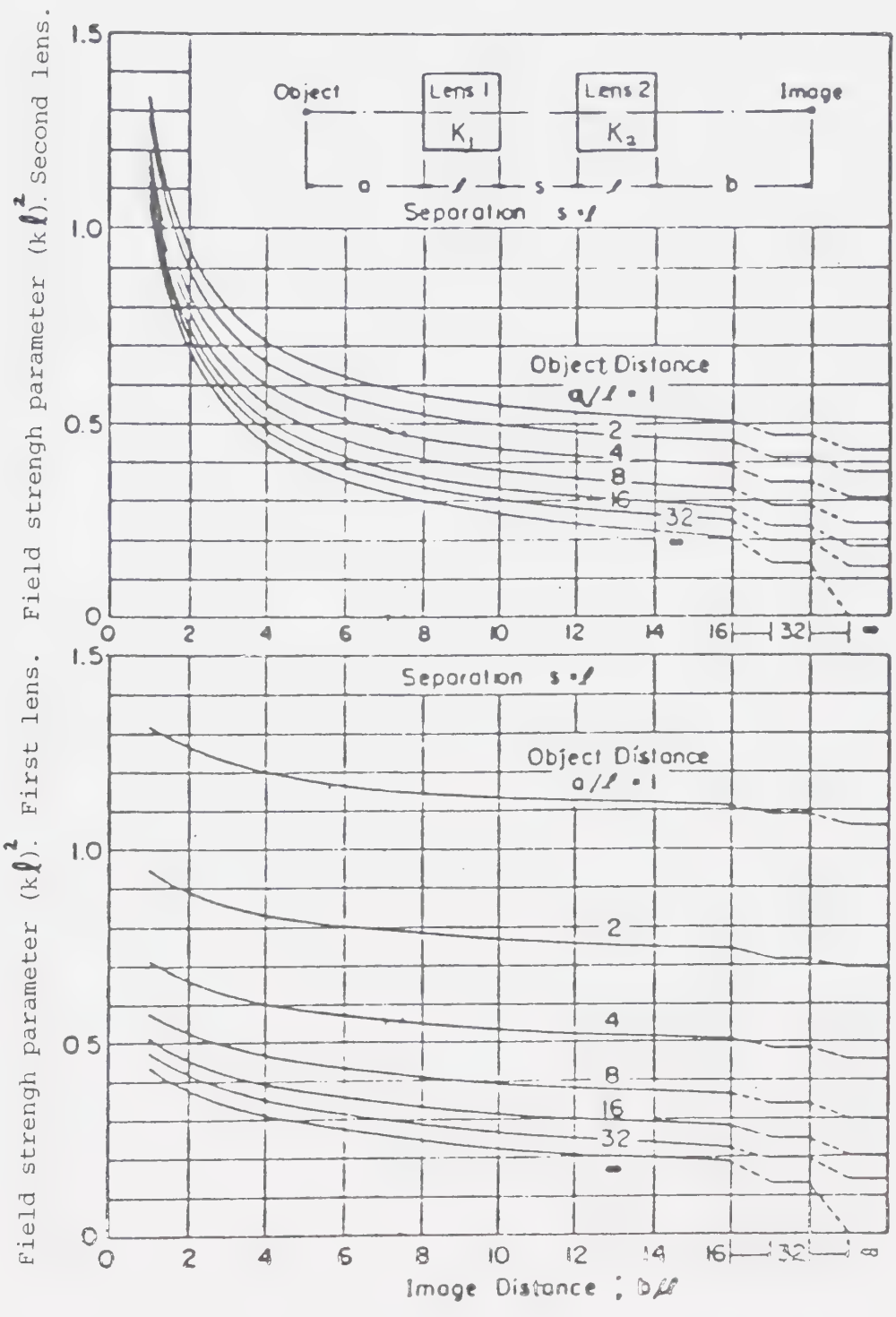

Figure 4.9 Field strength parameters vs. object and image distances for quadrupole lens pair of separation s = ℓ.

recording the high energy losses. However, if one wants to record and analyse a spectrum with energy loss as high as 2000 eV, one may require a detection system having a dynamic range of 10^8 and having a high DQE in this range, to resolve the ionization edges as illustrated in Fig. 1.2. These requirements can not be fulfilled by either serial or parallel detection systems alone. This may be one of the reasons why studies in the extreme high-energy-loss region of the spectrum have rarely been attempted.

It is clear that a SSD array parallel recording system has the fundamental advantage of a high DQE. This implies that it is most suitable for recording high energy losses, where the high collection efficiency of a parallel-recording device is most needed and where irradiation damage is less likely to be a severe problem because of the low intensities involved. To record the zero- and low-loss peaks, a second acquisition would be necessary, using a very low (10^{-12} - 10^{-13} A) current incident on the array, to avoid saturation. However, in the electron microscope it is difficult to control the beam current in this range. A very small condenser aperture could be inserted, but this would change the probe size at the specimen, and hence the area being analyzed. In the Conventional Transmission Electron Microscopy, a selected-area aperture could be employed and the second condenser lens used to control the electron current reaching the detector. But if the energy loss and collection angle are high, chromatic aberration of the

objective lens prevents the area of analysis being precisely defined.

An alternative solution is to use a serial detector to record the spectrum in the zero and low-loss region, where high collection efficiency is much less important than in the high-loss region. In this system, a serial detector will record the zero and low energy losses (up to 300 or 500 eV), while a parallel detector will record the high energy losses, within the range 300 or 500 eV to 2000 or 4000 eV. Thus the overall requirements for both dynamic range and DQE will be satisfied.

4.2.2 BASIC DESIGN

Figure 4.10 shows the basic design of a serial-parallel detection system. A photomultiplier/ scintillator combination is used as a serial detector since it offers good all-around performance (1.2.3). A SSD array is used as the parallel detector, exposed directly. The choice of a direct-exposure method is based on the following considerations. The DQE in the indirect-exposure system is typically less than 0.1. This situation can be improved by using an optical intensifier between the fluorescent screen and the array, but this presents more design problems, whereas a direct-exposure system has the advantages of high DQE and simplicity.

The energy resolution of a spectrum obtained with a parallel detector has to be considered in the design. As

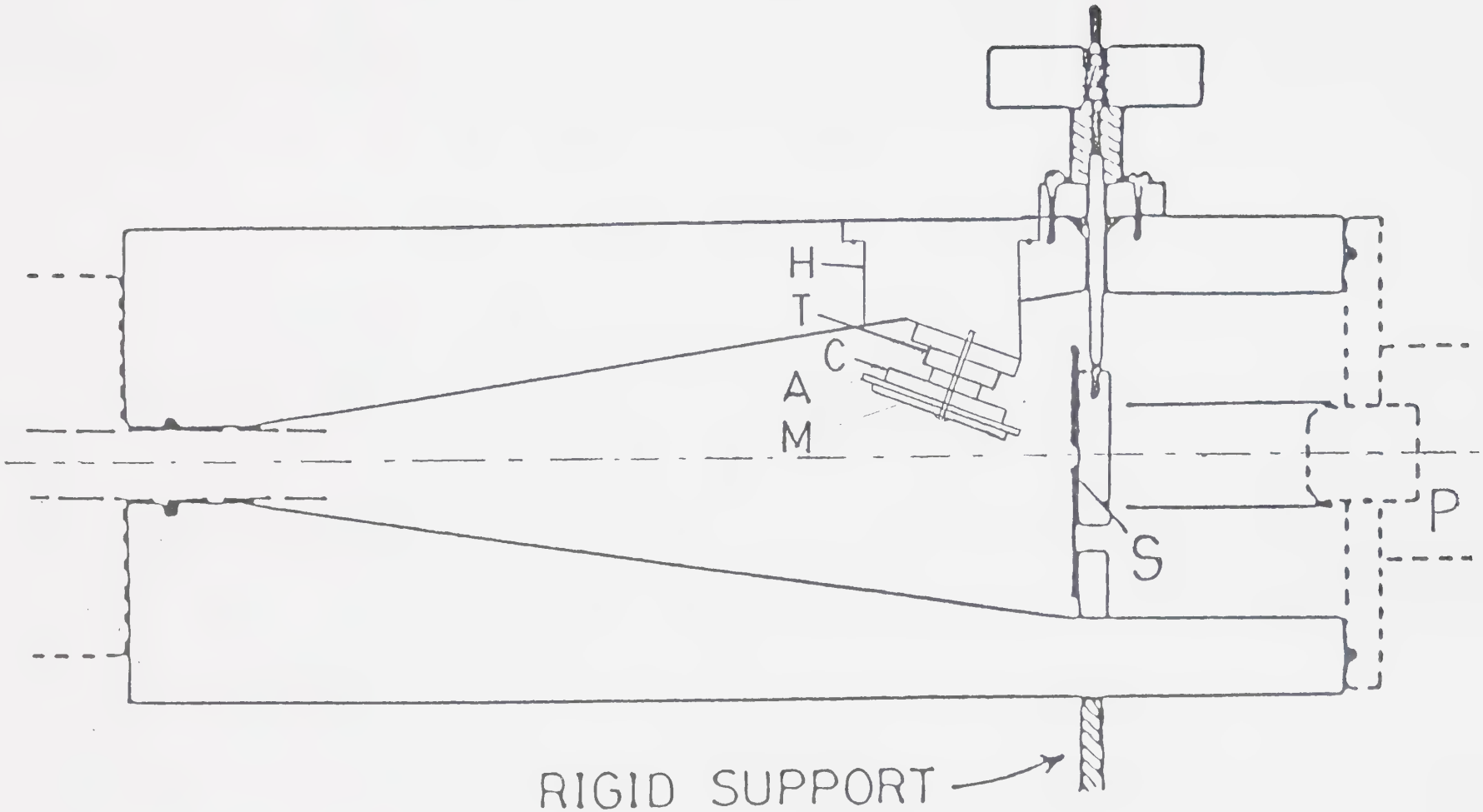

Figure 4.10 The design of a serial-parallel combination detection system.

mentioned in 4.1.1, while a SSD parallel detection system is used, the energy dispersion of the spectrum needs to be enlarged by a factor of 4 or 5. There are several ways to do this. One way is to use a post-spectrometer lens system as presented in 4.1. However, such a system is very inconvenient for the present purpose, because the image of the spectrum , after the post-spectrometer electron lens, is inverted. A slit has to be used for serial recording, and there will not be enough space between the image of the spectrum and the slit to install the SSD array together with its cooling device, as will be seen later. Thus the method adopted here to increase the energy dispersion is to tilt the SSD array by 70°. Using this method, an energy resolution of about 3 eV has been reported (Egerton 1981), a value which is acceptable in the present design.

Cooling the SSD array is important , as discussed in chapter 3. Our experiments (Egerton and Cheng 1982) have shown that a temperature of -30 °C to -40 °C increases the lifetime of an array significantly, as a result of reduced irradiation damage. A temperature lower than this might reduce the influence of irradiation damage even further. However the Reticon arrays used in this work are rated to -75°C(Reticon Corporation 1978). The use of very low temperature in the electron microscope might lead to gas condensation and eventual contamination of the array, depending on the quality of the vaccum. Therefore a working temperature of about -70 °C is to be achieved by using a

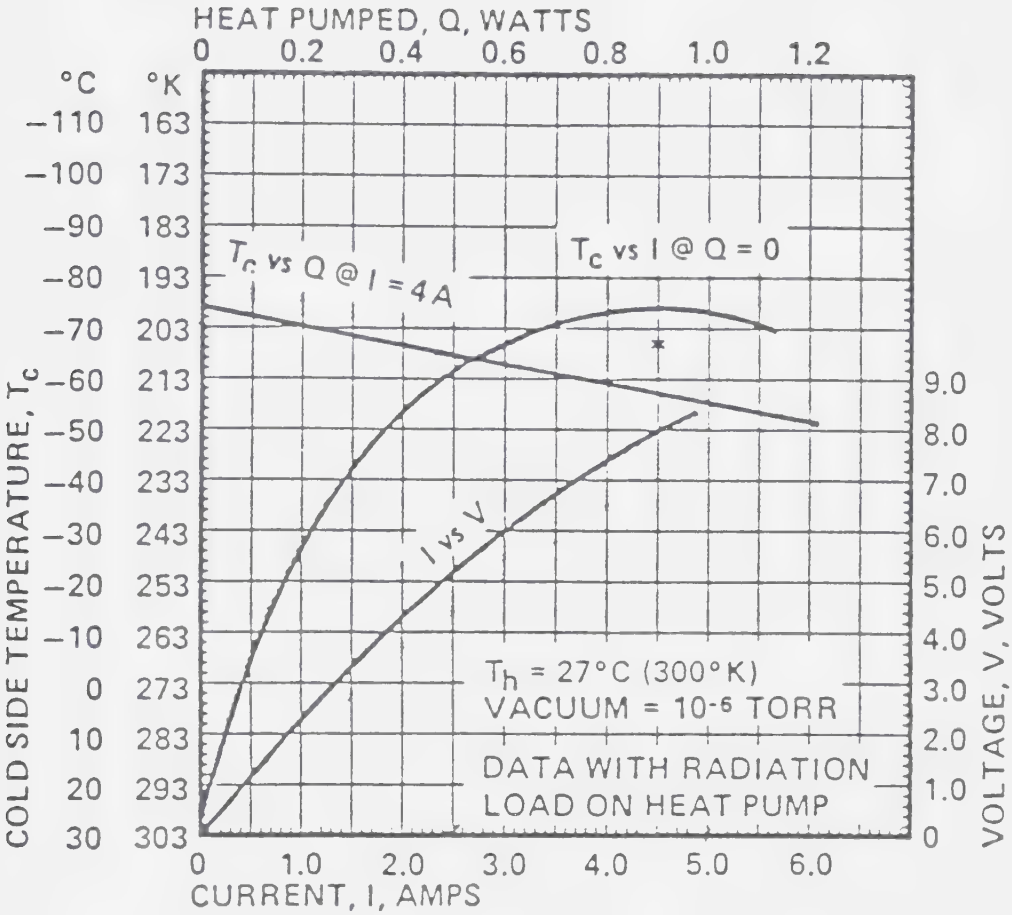

Figure 4.11 Characteristics curves of the thermoelectric device MI 3040.

cooling device.

The working temperature of an array, when it is attached to a cooling device, depends on both the power dissipation of the array and the characteristics of the cooling device. For a Reticon array, the DC power dissipation is 0.001 W and the maximum AC power dissipation is less than 0.1 W (Reticon Corporation 1978). For cooling, a thermoelectric device is under consideration since it has some advantages over liquid nitrogen. The choice of a thermoelectric device involves the requirements of working temperature (such as -70°C in this design), the geometry and the power of the cooler. A three stage thermoelectric device, model MI 3040 ,(MARLOW INDUSTRIES, INC), was finally chosen. Its characteristic curves are given in Fig. 4.11. It is seen from Fig. 4.11 that when a current of 4.5 Amps is used, the working temperature achieved for an array with power dissipation of 0.1 Watts is -70 °C.

The whole cooling-system design is shown in Fig. 4.10, where the hot side of the MI 3040 thermoelectric device is in contact with a heat sink made of copper metal.

CHAPTER V

CONCLUSIONS

An effective detection system in EELS must combine high collection efficiency, a large linear dynamic range and an immunity to beam-induced deterioration. A serial detection method, no matter how perfect the detector itself is, has a fundamentally poor detection quantum efficiency (DQE) because, out of the total of N channels, only one is being sampled at any given time. In a parallel detection method, the detector receives all the information simultaneously. Therefore, the DQE for a perfect parallel detector compared with that for a perfect serial detector (with N channels) will be enhanced by a factor of N. Hence a parallel detection system is in principle superior to a serial detection system.

Parallel recording systems using a semiconductor array as the detector retain the advantages of a photomultiplier and achieve simultaneous spectral measurement. These semiconductor array (SSD and CCD) can be exposed to an electron beam either directly or indirectly via a phosphor screen.

SSD arrays which are directly exposed to electrons have high DQE. At full output, the DQE is very close to unity. At the lower dynamic limit, DQE falls as the number of readouts increases, but, under typical conditions, DQE remains above

0.3. Therefore, in the direct-exposure mode, the array can behave as an almost ideal electron detector. The dynamic range of a cooled array (-30°C) at a single readout is only about 100, but increases almost linearly with readouts. With a large number of readouts, dynamic range in excess of 10^5 becomes possible. The major drawback of direct exposure to electrons is the problem of irradiation damage. The peripheral circuitry of an array can be protected from exposure to the incident high-energy electrons by a metal mask. However, under the bombardment of the electrons, radiation-induced space charge builds up in the array, increasing with the radiation dose received, and may finally saturate the array and make it useless. However, the effect of radiation damage depends on the temperature. It is found that the lifetime of an array, defined as the time taken for the output voltage to saturate when the incident-beam intensity is adjusted so that the video output amounts to half the maximum, is about 4 hours during continuous irradiation of 100 keV electrons at room temperature, but the estimated lifetime of the same array operated at -30°C is in excess of 1250 hours, which makes its operation promising. An even lower temperature might further reduce the irradiation damage and thus increase the lifetime of the array. Also, thermal annealing could restore an array which has suffered irradiation damage.

The indirect-exposure SSD array parallel detection system allows control over the detector sensitivity and

therefore an extension of the dynamic range. More importantly, it is free of the problems of radiation damage. However, all these advantages are obtained at the expense of reduced DQE, which is typically less than 0.3. This situation can only be improved by using an optical intensifier between the phosphor and the array, which will present more design problems.

A parallel detection system should be designed to give as good an energy resolution as possible within the limits of the energy spread imposed by the electron source. The simplest way of increasing the energy resolution is to tilt the array away from its normal incidence. An alternative way is to use a post-spectrometer lens system. An double symmetric magnetic lens gives a rotation-free image and the energy dispersion of the spectrum thus obtained is in fairly good agreement with the design. Calculations for a single quadrupole lens and a quadrupole double lens system show that they have a smaller power requirement compared with the double symmetric magnetic lens.

Although a parallel readout should allow a dynamic range in the recorded data of at least 10^5, the range of intensities within an energy-loss spectrum (from zero loss up to 4000eV) is larger than this. So a serial-parallel combination detecting system will probably be necessary. Direct-exposure parallel systems have a clear advantage in terms of simplicity and high DQE, and may be preferred for recording large energy loss, where the high collection

efficiency of a parallel-recording device is most needed and where irradiation damage is less likely to be a serious problem. This combination system will make possible the study of high energy losses, which should make a significant contribution to the development of EELS.

Bibliography

Autrata R., Schauer P. and Kvapil J. (1980), A single crystal of YAG-new fast scintillator in SEM, *J.Phys. E: Sci. Instrum.*, 11, 707-708.

Blasse G. and Brill A. (1967), A new phosphor-yellow emitting YAG, *Appl. Phys. Lett.*, 11, 53-55.

Chapman J. N., Glas F. and Roberts P. T. E. (1982), Two CCD-based detector systems for use in electron microscopy and related techniques, *Developments in Electron microscopy and Analysis*, 61, 131-134.

Comins N. R., Hengstberger M. M. E. and Thirlwall J. T. (1978), Preparation and evaluation of P-47 scintillators for a scanning electron microscope, *J. Phys. E: Sci. Instrum.*, 11, 1041-1047.

Cosslett V. E. and Thomas R. N. (1964), Multiple scattering of 5-30 keV electrons in evaporated metal films, *Brit. J. Appl. Phys.*, 15, 883-907.

Downing K. H., Ho M-H and Glaeser, R. M. (1980), A charge coupled device readout system for electron microscopy,

Proc. 38th Annual EMSA Meeting, Bailey G. W. (ed)(Claitors Press, Baton Rouge), 234-235.

Egerton R. F. and Kenway D. (1979), An acguisition, storage, display and processing system for electron energy loss spectra, *Ultramicroscopy*, 4, 221-225.

Egerton R. F. (1980), Instrumentation and software for energy loss microanalysis, *Scanning Electron Microscopy*, Johari O. (ed) 1, 41-52.

Egerton R. F.(1981a), Some general principles of EELS parallel detection, *Analytical Electron Microscopy*, Geiss R. H. (ed) (San Francisco press), 221-213.

Egerton R. F. (1981b), Design of a parallel detection system for EELS, *Proc. 39th Annual EMSA Meeting*, Bailey G. W. (ed) (Claitors Press, Baton Rouge), 368-369.

Egerton R. F. and Cheng S. C. (1982), The use of photodiode arrays to record 100 keV electrons, *J. Microsc.*, 127, RP3-RP4.

Enge H. A. (1959), Ion focusing properties of a quadrupole lens pair, *The Review of Scientific instruments*, 30, 348-351.

Everhart T. E., Wells O. C. and Oatley C. W. (1959), Wide band detector, *J. Electronics and Control*, 7, 97-111.

Farnell G. C. and Flint R. B. (1975), Photographic aspects of E.M., *Principles and Techniques of Electron Microscopy*, 5, Hayat M. A. (ed) (Von Nostrand Reinhold, NY), 19-61.

Fry P. W. (1975), Silicon photodiode array, *J. Phys. E*, 8, 337-350.

Gamble R. C. and Baldeschwieler J. D. (1979), Linear position-sensitive X-ray detector incorporating a self-scanning photodiode array, *Rev. Sci. Instrum.*, 50, 1416-1420.

Hall C. E. (1966), *Introduction to Electron Microscopy* 2nd, (McGraw-Hill Book Company, New York), 84-95; 129-132.

Hawkes P. W. (1970), *Quadrupoles in Electron lens Design* (Academic press, London), 144.

Horlick G. (1976), Characteristics of photodiode arrays for spectrochemical measurements, *Applied Spectroscopy*, 30, 113-123.

Jenkins D. G., Roussouw, Booker G. R. and Fry P. W. (1980),

Direct display of TEM images and EEL spectra using self scanned linear silicon photodiode arrays, *Institute of Physics Conference Series* **52**, Mulvey T. (ed), 81-84.

Johnson D. E., Monson K. L., Csillag S. and Stern E. A. (1981a), An approach to parallel detection EELS, *Analytical Electron Microscopy*, Geiss R. H. (ed) (San Francisco press), 205-209.

Johnson D. E., Csillag S., Monson K. L. and Stern E. A. (1981b), A photodiode parallel detection system,*Proc. 39th Annual EMSA meeting*, Bailey G. W. (ed) (Claitors Press, Baton Rouge), 370-371.

Jones B. L., Jenkins D. G., Booker G. R. and Fry P. W. (1977), Diode array detectors, *Institute of physics Conference Series* 36, 73-76.

Jones R. C. (1959), Quantum efficiency of detectors, *Adv. in Electronics and Electron Physics*, 11, 88-183.

Joy D. C. (1979), The basic principles of electron energy loss spectroscopy, *Introduction to Analytical Electron Microscopy* (Plenum press, New York), 223-244.

Joy D. C. and Maher D. M. (1980), The electron energy loss spectrum - facts and artifacts, *Scanning Electron*

Microscopy, Johari O. (ed)(SEM Inc., A. M. F. O'Hare, Illinois), 1, 25-32.

Killiany J. M. (1978), Radiation effect on sillicon charge-coupled devices, *IEEE Transaction on components, hybrids and manufacturing technology*, 4, 353-365.

Lowrance J. L. (1979), A review of solid state image sensors, *Advances in Electronics and Electron Physics* 52, 421-429.

Maher D. M. (1979), Elemental analysis using inner-shell excitations: a microanalytical technique for materials characterization, *Introduction to Analytical Electron Microscopy* (Plenum press, New York), 259-294.

Marlow Industries Inc. (1982), Guide to thermoelectric heat pumps, 1-17.

Mulvey T. (1982), Unconventional lens design in magnetic electron lenses, *Magnetic Electron Lenses*, Hawkes P. W. (ed) (Springer-Verlag Berlin), 370-375.

Oldham G., Ware A. R. and Salvaridis P. (1971), Radiation damage of organic scintillator materials, *J. Inst. Nuc. Eng.*, 12, 4-6.

Pawley J. (1974), Performance of SEM scintillation meterials, *Scanning Electron Microscopy*, 28-34.

Simpson R. W. (1979), Noise in large-aperture self-scanned diode arrays, *Rer. Sci. Instrum.*, 50, 732-732.

Shuman H. (1981), Parallel recording of EELS, *Ultramicroscoscopy*, 6, 163-168.

Shuman H., Somlyo A. V. and Somlyo A. P.(1981), Electron energy-loss analysis in biology: application to muscle and parallel collection system, *Microprobe analysis of biological systems*, Hutchnson T. E. and Somlyo A. P. (ed) 273-288.

Snow E. H., Grove A. S. and Fitzgerald D.J.(1967), Effects of ionizing radiation on oxidized silicon surfaces and planar devices, *Proceeding of the IEEE*, 55, 1168-1185.

Reticon Corporation (1982), S-series solid state line scanners (data sheet).

Roberts P. T. E., Chapman J. N. and Macleod A. M. (1982), A CCD-bassed image recording system for the CTEM, *Ultramicroscopy*, 8, 385-396.

Rose A. (1948), *Advances in Electronics*, Marton A. (ed)

(Academic, New York), 131.

Trebbia P., Ballongue P. and Colliex C. (1977), Data acquisition and handling for ELS, *Proc. 35th Annual EMSA Meeting*, Bailey G. W. (ed) (Claitors press, Baton Ronge), 232-233.

Wiggins J. W. (1978), The use of scintillation detectors in STEM, *proc. 9th Int. Cong. on EM*, Sturgess J. (ed), 1, 78-79.

Ximen, J. Y. (1979), Principles in electron optics, (Beijing University Press, Beijing), 84-88.